PD-1 Receptor Occupancy Assay for Mass Cytometry

Master Thesis in Medical Technology

Kristin Watnedal Olsen

Department of Chemistry,

UNIVERSITY OF BERGEN

Acknowledgment

Firstly, I would like to express my gratitude to my supervisor Bjørn Tore Gjertsen for giving me the opportunity to join this research group. Thank you for all the guidance and encouragement, and for always believing in me and this project. I want to send my deep and sincere gratitude to my supervisor Stein-Erik Gullaksen. You have been there every step of the way to teach and support me, always with patience and kindness. For that I am forever grateful. I also want to send my appreciation to my supervisor Svein Are Mjøs for valuable input and feedback.

Furthermore, I would also like to thank everyone in the Gjertsen Group for making me feel welcome and always helping me with both small and big challenges. I especially want to thank Reidun Kopperud, Øystein Sefland, Vibeke Andresen and Jørn Skavland for guidance with everything from cell culturing and experimental design to CyTOF and R. Additionally, I want to mention the lunch people whom I have had many interesting social conversations and insightful discussion with.

I am also grateful for my friends and family, who keep on supporting me in everything I do. Ann Linnea, thank you for always being there for me and giving me a feeling of home. I want to extend my greatest appreciation to my frisbee team for creating the ultimate space for my personal development, giving me valuable breaks, and making me more fit to handle all the challenges in the field of science.

Lastly, I want to thank my boyfriend Mathias Øgaard. No matter what happens, you always keep me down to earth.

Bergen, 2023

Kristin Watnedal Olsen

List of Content

List of Abbreviations

Abbreviation	Full name
ABC	Antibodies bound per cell
amu	Atomic mass units
CAS	Cell acquisition solution
CD	Cluster of differentiation
CDR	Complementary determining region
CM	Central memory
CSB	Cell staining buffer
EM	Effector memory
EMRA	Terminally differentiated effector memory
Fab	Fragment antigen-binding
Fc	Fragment crystallizable
FcγR	Fc gamma receptors
FCS	Flow cytometry standard
ICP-MS	Inductively coupled plasma mass spectrometry
ICP-OES	Inductively coupled plasma optical emission spectrometry
IgG	Immunoglobulin G
IgM	Immunoglobulin M
IgA	Immunoglobulin A
IgD	Immunoglobulin D
IgE	Immunoglobulin E
LAF	Laminar flow
mAbs	Monoclonal antibodies
mDC	Myeloid dendritic cell
MHC	Major histocompatibility complex
NK-cell	Natural killer cell
NKT	Natual killer T cell
NSCLC	Non-small cell lung cancer
PBLs	Peripheral blood leukocytes
PBS	Phosphate-buffered saline
PD-1	Programmed cell death receptor 1
pDC	Plasmacytoid dendritic cell
PD-L1	Programmed cell death ligand 1
PD-L2	Programmed cell death ligand 2
PFA	Paraformaldehyde
PHA	Phytohemagglutinin
PMA	Paramethoxyamphetamine
QSC	Quantum Simply Cellular
RCF	Relative centrifugal force
RECIST	Response evaluation in solid tumors
RO	Receptor occupancy
rpm	Revolutions per minute
RPMI	Roswell Park Memorial Institute
Tc	Cytotoxic T cell
Tdn	Double-negative T cell
Tdp	Double-positive T cell
Th	Helper T cell
TOF	Time of flight

Abstract

Pembrolizumab, a therapeutic antibody targeting PD-1, has shown great potential in treating various cancers, even giving durable responses for some patients. However, only a fraction of patients respond to this treatment. Today, the expression of PD-L1 on tumor cells is the most frequently used biomarker to predict response but it is still insufficient to use alone for most cancers. We hypothesized that the occupation by pembrolizumab on PD-1 could identify responders and non-responders. The single-cell analysis technology mass cytometry would enable investigation of occupation in complex cell types as it provides high sensitivity and detection of over 40 parameters. Therefore, we aimed to develop a PD-1 receptor occupancy assay for mass cytometry. A mass cytometry panel of antibodies was developed, containing 173Yb-anti-IgG4 [HP6025] to detect bound pembrolizumab and 166Er-anti-PD-1 [EH12.1] to detect available receptors not bound by pembrolizumab. The panel was tested on samples from 10 patients treated with pembrolizumab. Preliminary statistical analysis was conducted to investigate if there was a significant difference in receptor occupancy of responders and non-responders. The assay measured increasing PD-1 receptor occupancy by pembrolizumab in almost all patients. The results from the preliminary statistical analysis did not show any significant difference in the receptor occupancy of responders and non-responders, but more patients are required to assess this hypothesis. Nevertheless, as this assay enables the investigation of multiple cell populations simultaneously, it could still potentially contribute to predict response of pembrolizumab treated patients.

1 Introduction

1.1 Pembrolizumab

Pembrolizumab is a therapeutic antibody used in the treatment of various cancers. It blocks the function of a protein found on immune cells called programmed cell death receptor 1 (PD-1) that cancer cells exploit to evade the immune system, allowing the cancer cells to be attacked more easily (see Figure 1.1) [1]. Pembrolizumab was approved by the United States Food and Drug Administration in 2014 [2]. Today it is sold under the brand name Keytruda® and is used to treat multiple cancers. It is given as a monotherapy when treating melanoma, Hodgkin lymphoma, and urothelial cancer. For non-small cell lung cancer (NSCLC), head and neck squamous cell carcinomas, endometrial carcinoma, and renal cell carcinoma, it can be used as a monotherapy or in combination with other treatments. For esophageal, cervical, and triple-negative breast cancer, pembrolizumab is always combined with chemotherapy or other cancer treatments [3].

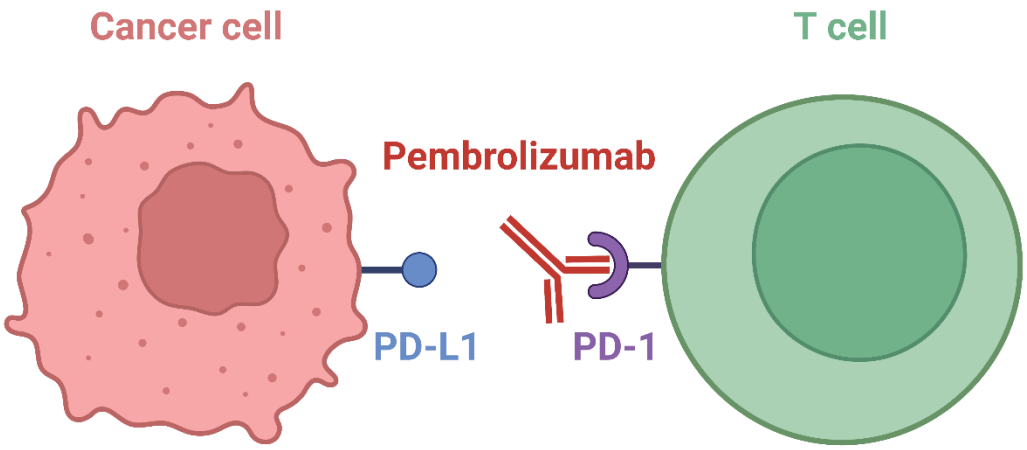

Figure 1.1 Mechanism of pembrolizumab. PD-1 on T cells is blocked by pembrolizumab, preventing PD-L1 on cancer cells from binding and suppressing the immune system. Pembrolizumab is, therefore, often referred to as a PD-1 inhibitor.

Pembrolizumab has been shown to be beneficial in treating several cancers, even giving durable responses in some cases [2]. However, not all patients respond to this treatment. The phase 1 study using pembrolizumab to treat patients with NSCLC only showed an objective response rate of 19,4 % [4]. Some patients also experience side effects, such as autoimmune reactions [5]. This demonstrates the importance of having predictive biomarkers to improve patient selection. Today, programmed cell death ligand 1 (PD-L1) expressed on tumor cells is the most common biomarker for predicting response to treatment with pembrolizumab. However, PD-L1 expression alone is often insufficient to predict response for most cancers [6]. Thus, the need for alternative strategies to predict the treatment response of pembrolizumab is evident. We hypothesized that measurement of PD-1 expression and its occupation by pembrolizumab could identify responders from non-responders.

1.2 Antibodies

Antibodies, or immunoglobulins, are Y-shaped proteins that are produced by B-cells. They help the immune system by binding to foreign pathogens to mark them for destruction by other immune cells [7]. There are five different isotypes of antibodies: IgG, IgM, IgA, IgD, and IgE. All these isotypes have similar but slightly different structures and functions [8]. IgG is the most abundant antibody in the blood, providing long-term immunity against various pathogens [9]. IgG is again divided into four subclasses: IgG1, IgG2, IgG3, and IgG4.

An antibody, shown in Figure 1.2, consists of four polypeptide chains: two heavy chains and two light chains [10]. An antibody's Fab (fragment antigen-binding) region comprises a constant and variable region from both the light and the heavy chain [11]. Within the variable region, there are three complementary determining region (CDR) loops. These loops determine the antibody's specificity and affinity upon binding to a receptor [12]. The region responsible for recognizing and binding to the receptors are called the paratope. Correspondingly, the part of the receptor that binds to the antibody is called the epitope [13]. The constant part of the Fab region is responsible for the stability and folding of the antibody [14].

The Fc (fragment crystallizable) of the antibody, on the other hand, is responsible for the antibody's effector functions. The region consists of two heavy chains that can interact with other components of the immune system [11]. These interactions can trigger responses from the immune system, such as phagocytosis or antibody-dependent cellular cytotoxicity. The Fc region can also activate complement, a group of proteins that help destroy pathogens [15]. Pembrolizumab is an example of an IgG4 antibody that has been humanized, meaning that CDRs from a non-human host has been integrated in a human antibody. This process is referred to as CDR-grafting [16].

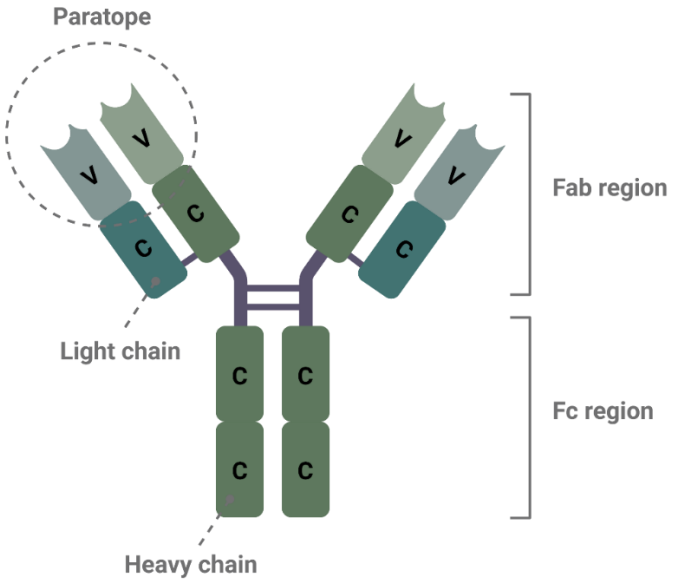

Figure 1.2 Structure of a typical IgG antibody. The structure is divided into a Fab and an Fc region. There are two heavy chains and two light chains, each containing constant and variable regions. The paratope is located at the variable regions of the antibody.

1.3 T cells

T cells are white blood cells that play a vital role in the immune system. They are responsible for attacking infected cells and regulating the immune response. T cells are produced in the bone marrow and then matured into cytotoxic-, helper- or regulatory T cells in the thymus gland [7]. Cytotoxic T cells (Tc), or $CD8^+$ T cells, attack and kills infected cells [17]. Helper T cells (Th), or $CD4^+$ T cells, can activate and coordinate the immune response towards a cytotoxic T cell or B-cell response [18]. Regulatory T cells can regulate the other T cells' activity and response, thereby suppressing the immune response [19]. This is essential to prevent autoimmunity, where T cells start attacking healthy cells. Some T cells are positive for both the CD4 marker and the CD8 marker. These are called double-positive T cells (Tdp) [20]. Correspondingly, there exist T cells that do not express CD4 or CD8 on their cell surface, referred to as double-negative T cells (Tdn) [21].

T cells have receptors on their surface that can bind to and recognize antigens, peptides presented on the surface of other cells or pathogens by a major histocompatibility complex (MHC) protein [22]. If the antigen presented to the T cell is recognized as foreign, it activates and triggers an immune response. Then the T cells will multiply and migrate to the site of the foreign antigen, where they start to attack and kill the infected cells [9].

The different types of T cells can be characterized as naïve T cells or memory T cells. Naïve T cells have not yet encountered a foreign antigen. In contrast, memory T cells have previously been exposed to a foreign antigen and can therefore be more effective in the response against the same type of infected cells [23]. Furthermore, memory T cells are commonly divided into effector memory T cells (T_{EM}) or central memory T cells (T_{CM}). Effector memory T cells (T_{EM}) can migrate to inflamed peripheral tissue and have an immediate effector function. Central memory T cells (T_{CM}) can migrate to secondary lymphoid organs and do not have a quick effector function. However, if these cells are stimulated with an antigen, they become activated and differentiate into an effector cell [24].

1.4 Programmed Cell Death Receptor 1

Programmed cell death receptor 1 (PD-1) is a cell surface protein that regulates immune response. The receptor is mainly expressed on the surface of T cells and B-cells upon activation [25]. The PD-1 receptor belongs to the immunoglobin family and is a type 1 transmembrane protein [26]. It consists of an extracellular, a transmembrane, and a cytoplasmic domain. The extracellular domain has a structure similar to the variable domain of an antibody and is separated from the plasma membrane by a stalk of around 20 amino acids [27]. This domain consists of a variable and a constant part and is responsible for binding the receptor to its ligands. This extracellular domain is followed by a transmembrane domain and, lastly, a cytoplasmic tail containing two tyrosine-based residues [28].

PD-1 usually binds to one of its ligands: programmed cell death ligands 1 and 2 (PD-L1 and PD-L2). PD-L1 is usually expressed on B and T cells, dendritic cells, and macrophages, while PD-L2 is expressed on activated macrophages and dendritic cells [29]. Upon binding to PD-L1 or PD-L2, the two tyrosine residues on the cytoplasmic tail become phosphorylated. This leads to the recruitment of phosphatases, which further causes the dephosphorylation of signaling

molecules involved in T cell activation, proliferation, and cytokine production [27]. As a result, T cell activation and proliferation are inhibited while T cell exhaustion and apoptosis are induced [30]. Thus, the PD-1 receptor acts as a negative regulator of the immune response, maintaining immune tolerance and preventing autoimmunity. Some tumor cells have increased PD-L1 expression, which allows them to go undetected by the immune system [31]. Therefore, it has been shown that elevated expression of PD-L1 on tumor cells is often correlated with poor disease prognosis [32]–[39].

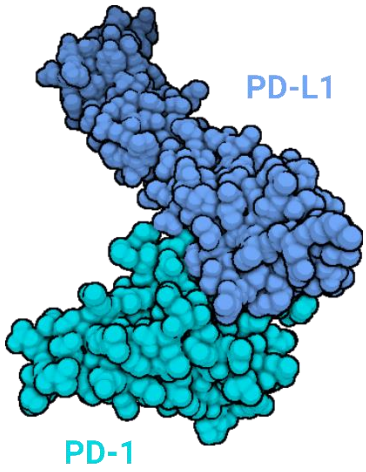

Figure 1.3 The crystal structure of PD-L1 bound to PD-1. The structure was mapped using X-ray crystallography at a resolution of 2,65 Å by Lin et al. (2008) [40]. The structure was retrieved from The Protein Data Bank (PDB ID: 3BIK), and the figure was created with Biorender.

The crystal structure of PD-1 bound to PD-L1, shown in Figure 1.3, has been uncovered by Lin et al. (2008) using X-ray crystallography [40]. Later, the structure was also mapped by Zak et al. (2015) [41]. This revealed that the variable and constant domains form a flat binding surface on the PD-1 receptor and that several hydrogen bonds, salt bridges, and hydrophobic interactions are involved in the binding to PD-L1. Similarly, the crystal structure of pembrolizumab in complex with PD-1, shown in Figure 1.4, has been reported by several groups [42]–[44]. The findings in these papers all indicate that the epitope on PD-1 that recognizes pembrolizumab largely overlaps with that of PD-L1. This suggests that the mechanism of pembrolizumab is to occupy the epitope of PD-L1, leading to steric hindrance that will prevent PD-L1 from binding to PD-1 [45].

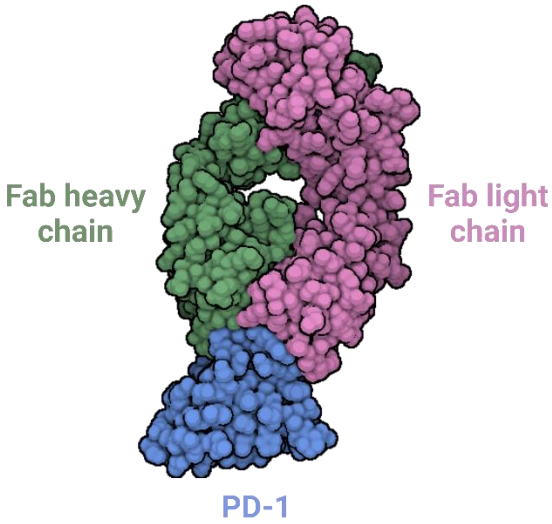

Figure 1.4 The crystal structure of PD-1 (blue) in complex with the Fab region of pembrolizumab (pink and green). The structure was mapped by Na et al. (2017) using X-ray crystallography at a resolution of 2,90 Å [42]. The structure was retrieved from The Protein Data Bank (PDB ID: 5JXE), and the figure was created with Biorender.

1.5 Cytometry

Cytometry refers to the quantitative analysis of single cells. The field of cytometry consists of various techniques, most of which detect molecular properties of cells or cell systems [46]. Today, one of the most well-established methods is flow cytometry, but more recent methods like mass cytometry are also emerging in the field.

1.5.1 Flow Cytometry

Flow cytometry is a laser-based technology that allows for the simultaneous analysis of multiple parameters on single cells. In a flow cytometry experiment, single-cell suspension cells are incubated with fluorochrome-labeled antibodies binding to specific proteins expressed on cells. This allows the fluorochrome-labeled antibodies to serve as reporters for the protein expression on a single cell, which can provide information about the cell type or cellular processes. After the incubation, the single-cell suspension is introduced into a flow cytometer where the cells pass through a focused laser beam, one cell at a time [47]. This creates light scatter that is detected by different detectors. The visible light scatter gets detected in two directions: forward and sideways. Forward scatter indicates the cell's size, while side scatter is correlated with the cell's internal complexity or granularity [48]. The fluorochromes, conjugated to antibodies, also emit light at specific wavelengths due to being excited by the laser. The emitted light at each wavelength is detected by distinct channels. When several fluorochromes are used, there is usually some overlap between them as each of them have wide emission spectra [49]. Every cell that passes through the flow cytometer is detected as a single event. Each event contains data on the emitted light signal intensity in each channel [50]. These data are saved in a .FCS-file that can further be analyzed [48].

1.5.2 Mass Cytometry

Mass cytometry is a single-cell analysis technology using inductively coupled plasma mass spectrometry (ICP-MS) and enables the quantification of more than 40 cellular parameters. In a mass cytometry experiment, cells are incubated with metal-labeled antibodies that can bind to targets within or on the surface of a cell [51]. Mass spectrometry allows for the detection of metal isotopes through different mass channels that can distinguish the different isotopes with high accuracy and little signal overlap [52]. This allows the measured abundance of metal isotopes to serve as reporters for the expression of proteins on single cells. The resolution and the high throughput make mass cytometry an ideal technology for analyzing complex cellular systems [53].

A regular process of a mass cytometry experiment starts with collecting samples, such as blood, bone marrow, or biopsy. Any additional processing or treatment of the samples is then carried out, followed by fixation to preserve the state of the cells [54]. Samples can further be barcoded using a unique combination of heavy metals to enable the pooling of all the samples. This is usually done to reduce technical variability and workload in further processing [55]. The next step is staining, where the pooled sample is incubated with a mix of antibodies. This step can also be done before fixation, referred to as live cell staining. The antibodies used for staining have previously been conjugated to chelating polymers with specific heavy metal isotopes attached [56]. Cells are first stained with extracellular antibodies, which recognize targets on the cell surface. If intracellular targets are of interest, the cells can be permeabilized and stained with intracellular antibodies afterward [51].

Figure 1.5 shows an overview of the workflow in mass cytometry. First, the sample is introduced to the mass cytometer through a nebulizer in which the cell suspension is converted to a spray of droplets containing single cells [57]. A flow of make-up gas transfers the droplets through a heated spray chamber, where the water evaporates [54]. The cells then enter the inductively coupled plasma (ICP) torch, where they pass through an argon plasma with a temperature of approximately 7000 K [6]. The argon plasma breaks the sample into constituent elements and ionizes the metals [57]. The produced ion cloud then enters a quadrupole which removes ions with a molecular weight lower than approximately 75 amu. This efficiently removes most of the ions from the cell itself (C, N, O etc.) and retains any heavy metals that were conjugated to a cell bound antibody. The metal ions then pass through to the time of flight (TOF) analyzer [51]. Here, an electric field accelerates the ions, and their flight times are recorded. The flight times of the ions will depend on their mass to charge ratio, which is specific for each isotope. When the ions hit the detector, they create an electric pulse. These pulses are converted to dual counts. For low ion concentrations, the resulting pulses is directly recorded as dual counts. For higher ion concentrations, the pulses are adjusted with a coefficient due to an overlap in the intensity distributions of the pulses [54]. The dual count from the pulses can then be paired with specific isotope tagged antibodies. Integrated signals for every single cell are compiled into a .FCS-file, which can further be analyzed [53].

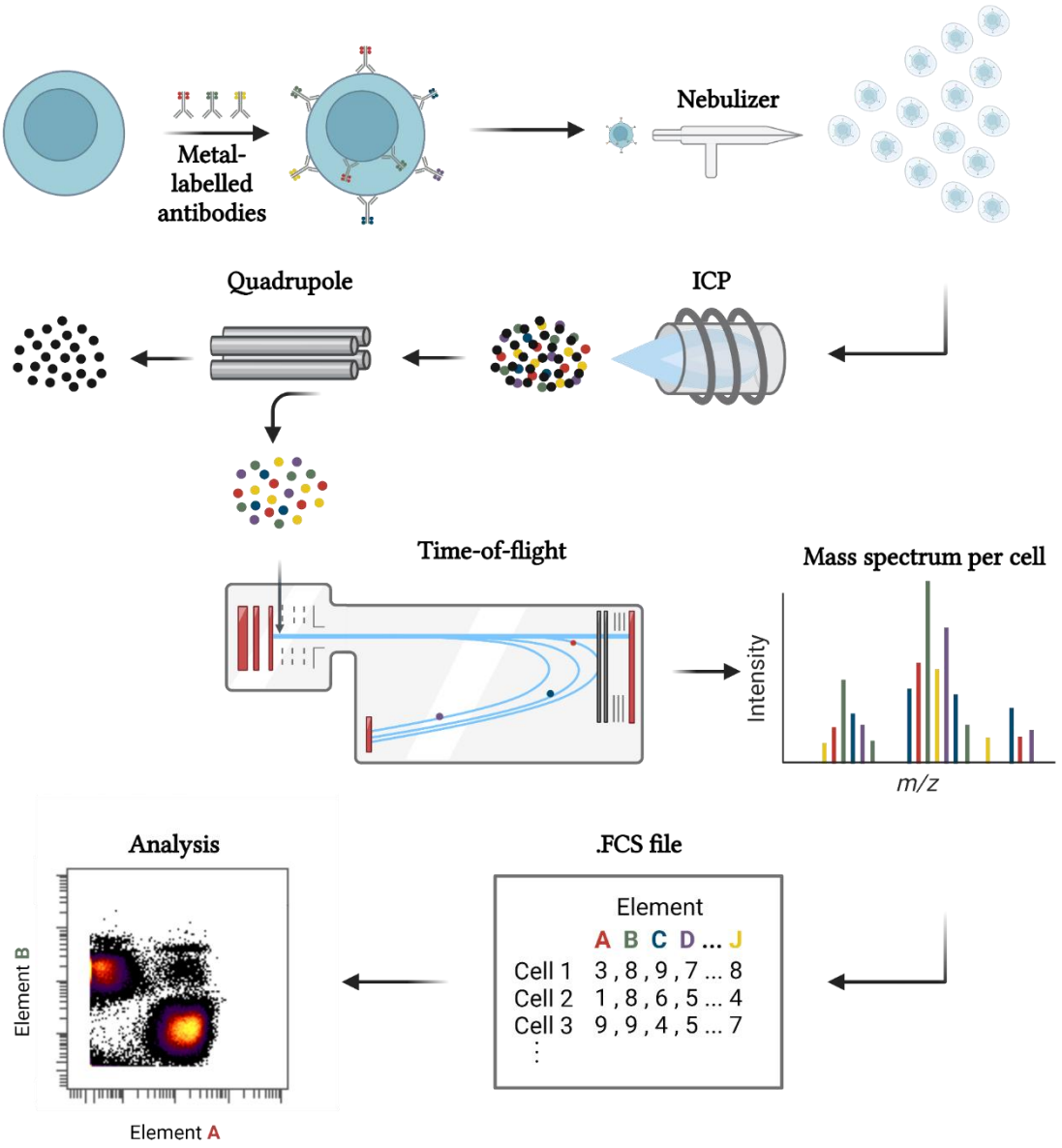

Figure 1.5 Overview of the workflow in mass cytometry. Cells are first stained with metal-labeled antibodies before being injected into the nebulizer. The resulting droplets get ionized in the ICP torch, and biological elements are removed by the quadrupole. The metal ions are detected in a time-of-flight analyzer, which results in a mass spectrum per single cell. This is converted into an. FCS file for further analysis. The figure is adapted from [53].

1.6 Receptor Occupancy

1.6.1 Concept

Receptor occupancy refers to the degree to which a cells receptors are saturated by its ligands. This concept was first proposed in 1900 by Paul Ehrlich, who suggested that the effect of a drug is proportional to the amount of drug that occupies its receptors [58]. Anti-PD-1 drugs seem to

follow this relation, according to Cowles et al. (2022). They also found that the slow internalization rate and low antigens concentration allow anti-PD-1 antibodies to fully saturate the receptors. Therefore, the saturation is mainly limited by the clearance rate of the drug [59]. These findings indicate that receptor occupancy could serve as a reporter of drug efficacy and predict drug response for patients receiving treatment with PD-1 inhibitors.

Generally, there are four types of assays to measure receptor occupancy (three assays illustrated in Figure 1.6): free receptors, total receptors, bound receptors, and receptor modulation. Measuring free receptors is an indirect determination where a competitive antibody or labeled drug is used to identify the receptors not blocked by the drug. The assay of total receptors uses a non-competitive antibody in the presence or absence of the drug to determine the total amount of receptors available. This method can also be combined with a competitive antibody or a labeled drug to determine both total receptors and free receptors at the same time. Bound receptors refer to the detection of bound drugs using an anti-drug antibody. Lastly, the receptor modulation assay monitors the functional effect caused by the binding to assess receptor occupancy [60]. The resulting receptor occupancy can be expressed as a relative frequency, either as a percentage or an absolute cell count or by antigen expression quantified by an antigen quantitation bead or cell reference control [61].

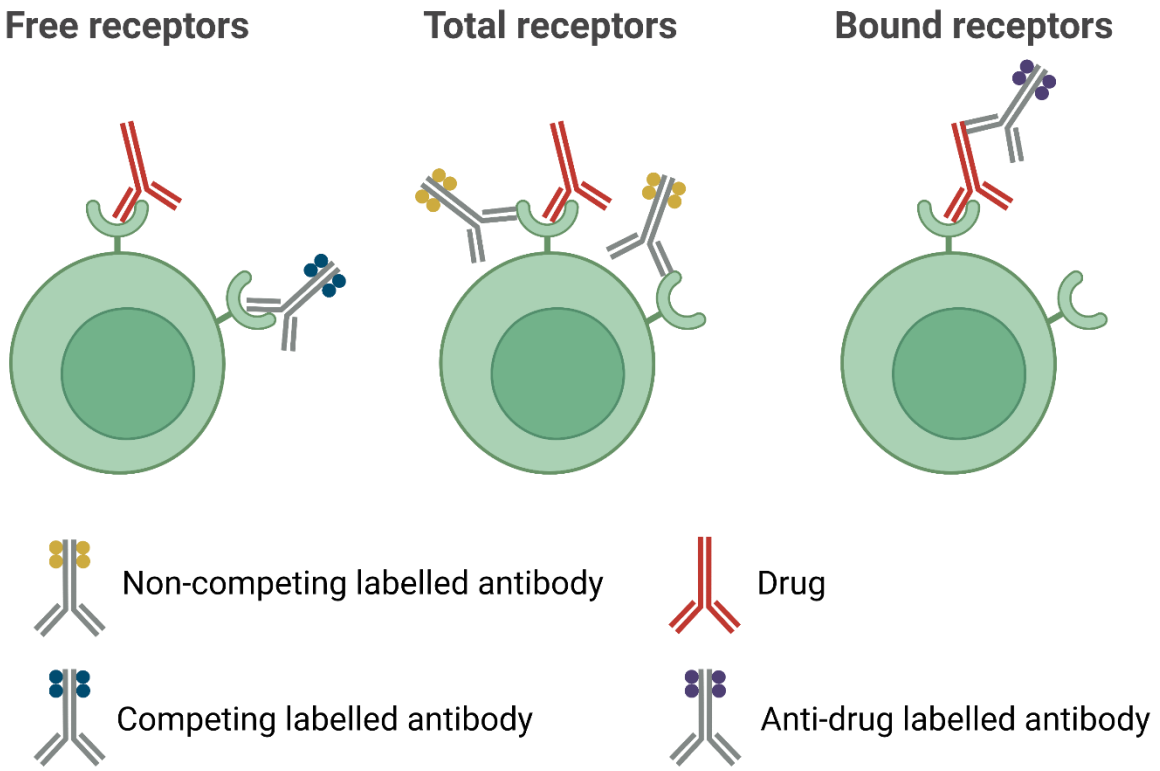

Figure 1.6 Three assays for measuring receptor occupancy. The free receptor approach uses a competing labeled antibody to detect unoccupied receptors. The total receptors approach is based on a non-competing labeled antibody detecting all available receptors. The approach of bound receptors measures bound drugs with an anti-drug labeled antibody. Figure inspired by [62].

1.6.2 Receptor Occupancy in Flow Cytometry

Receptor occupancy assays are already well established in flow cytometry. In 2010, a bound receptor assay was used in the phase I study of nivolumab, another PD-1 inhibitor that has partially overlapping epitope with pembrolizumab [63]. Since then, several bound receptor strategies for determining the receptor occupancy of PD-1 inhibitors have been described [64]–[66]. All these assays use an anti-IgG4 secondary antibody that binds to the constant part of human IgG4 antibodies. As nivolumab is a fully human IgG4 antibody and pembrolizumab is a humanized IgG4 antibody, this allows for the detection of bound nivolumab and pembrolizumab on the cell surface. More recently, Osa et al. (2018) developed an assay using the combination of bound receptors, detected by an anti-IgG4 secondary antibody, and free receptors, detected by a competing labeled anti-PD-1 antibody (clone: EH12.1) [67]. Herein, the patient binding status was divided into complete, partial, or no binding by comparing the levels of bound and free receptors before and after receiving treatment with nivolumab. This approach was also used by Osa et al. (2019) to determine the receptor occupancy of pembrolizumab and later by Gazanno et al. (2022) to check if receptor occupancy is associated with immune-related adverse events in patients receiving anti-PD-1 treatment [68], [69].

All but one of the assays described in the previous paragraph stain the cells with the antibodies while the cells are alive. The advantage of this is that the cell environment is more similar to that in the patient, but this also requires the samples to be stained and analyzed shortly after sample acquisition. Sometimes cryopreservation, cooling the cells to very low temperatures, is necessary, for example, in the batch analysis of clinical trials [65]. Then, the cells can first be fixed to stabilize the cell and preserve their structure during freezing and thawing. This includes keeping drugs attached to the cell surface receptors throughout the process. Pluim et al. (2019) used cells fixed with 2 % formaldehyde before staining them with an anti-IgG4 secondary antibody to determine bound nivolumab and pembrolizumab. To my knowledge, this is the only receptor occupancy assay for anti-PD-1 drugs using fixed cells. This shows significant unexplored potential for developing a PD-1 receptor occupancy assays for fixed cells.

1.6.3 Receptor Occupancy in Mass Cytometry

Mass cytometry is another technology that could serve as an alternative in measuring receptor occupancy. Instead of fluorophore-labeled antibodies, mass cytometry uses metal-labeled antibodies as described previously. Huse, Kanutte (2019) states this about the advantages of using mass cytometry in receptor occupancy assays: “Mass cytometry would further expand the possibilities to measure receptor occupancy of complex cell types as metal-labeled antibodies and minimal overlap between channels allow for more than 40 markers to be detected simultaneously without loss of sensitivity” [62]. Although mass cytometry could serve as a valuable tool in receptor occupancy assays, there are some challenges regarding the sensitivity of the mass channels used to detect the conjugates antibodies. Each channel has different sensitivity, resulting in different signal for each detected antibody. Thus, comparing the signal of an anti-PD-1 antibody and a secondary anti-drug antibody could result in inaccurate receptor occupancy calculations.

In 2019, Bringeland et al. used mass cytometry for a receptor occupancy assay, measuring natalizumab bound to its receptor integrin by a bound and total receptor approach [70].

Quantum™ Simply Cellular® (QSC) beads were used to standardize the signals across channels. These beads bind an exact number of antibodies to their surface. This can be used to generate a standard curve for the mass channel, making the receptor occupancy estimates more accurate. Another solution to the same standardization issue was proposed by Stevens et al. (2023) [71]. Here, standard curves of each metal were made with inductively coupled plasma optical emission spectrometry (ICP-OES) to determine the mean amount of metal on each antibody. Then by measuring the signal of metal on a single cell, this number could be converted to the number of antibodies bound per cell (ABC). These standardization techniques could overcome the problem of inaccuracy due to the mass channels, establishing mass cytometry as a valuable tool for determining receptor occupancy. Although mass cytometry has previously been used to assess receptor occupancy, it has never been explicitly used for the receptor occupancy of anti-PD-1 drugs, including that of pembrolizumab.

2 Aims

The main aim of this thesis was to develop an assay that could measure the receptor occupancy of pembrolizumab using mass cytometry. The ultimate goal is to test if this assay can contribute to response prediction in patients treated with PD-1 inhibitors. The specific objectives of the Master thesis are as follows:

1. Adapt an in-house developed mass cytometry panel of antibodies to detect pembrolizumab and PD-1 on the cell surface of T cells, including validation of antibodies detecting pembrolizumab and PD-1.
2. Determine if the receptor occupancy of PD-1 can be calculated in samples from patients receiving treatment with pembrolizumab.
3. Test if the calculated receptor occupancy can be used as a predictor for pembrolizumab treatment effect.

3 Materials and Methods

3.1 Panel

3.1.1 Panel Development

A mass cytometry panel developed in-house by PhD Reidun Kopperud was used as the starting point for the work conducted in this thesis. This panel was further developed to fit the investigative purpose of the thesis. The final panel comprises 29 extracellular antibodies (see Table 3.1) and 8 intracellular antibodies (see Table 3.2). The extracellular antibodies were mainly used for immunophenotyping and assessing receptor occupancy, while the use of intracellular antibodies aimed to reveal signaling effects. Even though investigating any signaling effects is not addressed in this thesis, the intracellular markers were still included to generate signaling data that could be analyzed in the future. Some antibodies were tested and used in some of the experiments described later but were rejected for use in the final panel. These antibodies can be found in Table 3.3.

Table 3.1 Extracellular Antibody Panel. Overview of all extracellular antibodies in the final panel showing the target of the antibody, the clone, the isotope, and corresponding metal conjugated to the antibody, and the company supplying the antibody with the corresponding product number.

Extracellular Antibody Panel					
Isotope	**Metal**	**Target**	**Clone**	**Company**	**Product number**
89	Y	CD45	HI30	Fluidigm	3089003B
111	Cd	CD3	UCHT1	BioLegend	300443
112	Cd	CD123	6H6	BioLegend	306027
114	Cd	CD66b	G10F5	BioLegend	305102
116	Cd	HLA-DR	L243	BioLegend	307651
139	La	CD1c	L161	BioLegend	331502
141	Pr	CD141	501733	Invitrogen	MA5-24214
142	Nd	CD57	HCD57	Fluidigm	3142007B
143	Nd	CD45RA	HI100	Fluidigm	3143006B
145	Nd	CD4	RPA-T4	Fluidigm	3145001B
146	Nd	CD45RO	UCHL1	BioLegend	304239
147	Sm	CD20	2H7	Fluidigm	3147001B
148	Nd	CD16	B73.1	BioLegend	360702
149	Sm	CD25	2A3	Fluidigm	3149010B
152	Sm	CD107a	H4A3	BioLegend	328635
154	Sm	TIM-3	F38-2E2	Fluidigm	3154010B
157	Gd	CD8a	HIT8A	BioLegend	300902
158	Gd	CD27	L128	Fluidigm	3158010B
160	Gd	CD14	RMO52	Fluidigm	31600B
163	Dy	CD56	NCAM16.2	Fluidigm	3163007B
164	Dy	CD161	HP-3G10	Fluidigm	339919
166	Er	CD279 (PD-1)	EH12.1	BD Biosciences	562138
169	Tm	ICOS	C398.4A	Fluidigm	3169030B
171	Yb	NKp46	9E2	BioLegend	331902
172	Yb	CD38	HIT2	Fluidigm	3172007B
173	Yb	IgG4	HP6025	Invitrogen	A10651
174	Yb	CD11c	Bu15	BioLegend	337221
175	Lu	PD-L1	29E.2A3	Fluidigm	3175017B
209	Bi	TIGIT	MBSA43	Fluidigm	3209013B

Table 3.2 Intracellular Antibody Panel. Overview of all intracellular antibodies in the final panel showing the target of the antibody, the clone, the isotope and corresponding metal conjugated to the antibody, and the company supplying the antibody with the corresponding product number.

Intracellular Antibody Panel					
Isotope	**Metal**	**Target**	**Clone**	**Company**	**Product number**
144	Nd	pTYR	Tyr100	Fluidigm	314400A
150	Nd	pSTAT5 [Y694]	47	Fluidigm	3150005A
151	Eu	pSTAT3 [S727]	D4X3C	CST	624084
153	Eu	pSTAT1 [Y701]	58D6	Fluidigm	3153003A
156	Gd	p-p38 [T180Y182]	D3F9	Fluidigm	3156002A
161	Dy	T-bet	4B10	Fluidigm	3161014B
162	Dy	Ki-67	B56	Fluidigm	3162012B
165	Ho	pCREB [S133]	87G3	Fluidigm	3165009A

Table 3.3 Tested Antibody Panel. Overview of tested antibodies that were not included in the final panel but were used in some experiments. The table shows the target of the antibody, the clone, the isotope and corresponding metal conjugated to the antibody, and the company supplying the antibody with the corresponding product number.

Tested Antibodies					
Isotope	**Metal**	**Target**	**Clone**	**Company**	**Product number**
159	Tb	CD279 (PD-1)	Pembrolizumab	Merck	J9271
168	Er	CD279 (PD-1)	MIH4	Invitrogen	14-9969-82
176	Yb	CD279 (PD-1)	EH12.2H7	Invitrogen	329902

3.1.2 Conjugation of Antibodies

Conjugation refers to the process in which a metal becomes chelated to a polymer, which then gets conjugated to an antibody. Some antibodies used in the panel were already pre-conjugated by the manufacturer, but some antibodies needed to be conjugated in-house. This was done by using Maxpar® X8 Polymer Labeling Kits and following the corresponding protocol provided by Fluidigm (South San Francisco, CA, USA). This conjugation procedure involves loading an X8 polymer with a lanthanide metal solution simultaneously as partially reducing the antibody. Then the antibody becomes conjugated with the lanthanide-loaded polymer. After conjugation, a NanoDrop spectrophotometer was used to measure the concentration, giving the yield of the process. In-house conjugated antibodies and their respective yield is shown in Table 3.4.

Table 3.4 Yield of in-house conjugated antibodies. Showing yield value of conjugation as a percentage of the original amount of antibody being conjugated.

The yield of in-house conjugated antibodies				
Isotope	**Metal**	**Target**	**Clone**	**Yield (%)**
151	Eu	pSTAT3 [S727]	D4X3C	72
159	Tb	CD279 (PD-1)	Pembrolizumab	107
166	Er	CD279 (PD-1)	EH12.1	89
168	Er	CD279 (PD-1)	MIH4	98
173	Yb	IgG4	HP6025	74
174	Yb	CD11c	Bu15	69
176	Yb	CD279 (PD-1)	EH12.2H7	101

3.1.3 Titration of Antibodies

A titration of all in-house conjugated antibodies and new pre-conjugated antibodies from the manufacturer is necessary to determine the optimal concentration of the antibody in the panel. There are some important factors to consider in conjugation. First, the signal of the antibody to needs to be high enough to clearly distinguish populations that express the antibody target from those that do not. But the antibody concentration should not be too high as this can lead to unspecific binding. Another factor to consider is that if one can get satisfactory separation with a lower antibody concentration, you will save both antibodies and money.

In-house conjugated, and new pre-conjugated antibodies were titrated on lysed and fixed cells from healthy donor peripheral blood. Titration was done as described by Gullaksen et al. (2019) [72]. Herein, cells were stained with a backbone panel in addition to a serial dilution of the antibodies to be titrated. The backbone panel was a selection of the most important immunophenotyping antibodies from the in-house developed panel. All the antibodies already had pre-determined optimal concentrations used in the titration. The titrated cells were run on CyTOF XT® (Fluidigm, South San Francisco, CA, USA), and the titration results were assessed using Cytobank.org [73].

3.2 Cell Lines

3.2.1 Cell Culturing

Jurkat (Clone E6-1), a clone established from the peripheral blood of a 14-year-old male with acute T cell leukemia was purchased from American Type Culture Collection (Manassas, VA, USA). Cells were cultured in Roswell Park Memorial Institute (RPMI)-1640 medium (Merck KGaA, Darmstad, Germany) supplemented with 10% fetal bovine serum (VWR International, Radnor, PA, USA), 1% penicillin/streptomycin (Merck KGaA, Darmstad, Germany) and 1% L-glutamine (Merck KGaA, Darmstad, Germany). The cell cultures were kept in a humidified incubator at 37°C with 5% CO_2. The concentration of cells was kept within 0,3-2,0×10^6 cells/mL by changing the medium every 2-3 days. Cells were counted using a Countess™ 3 Automated Cell Counter. All cell culture work was done in a sterile laminar flow (LAF) bench containing a high-efficiency particulate air filter.

3.2.2 Thawing Cells

Cryopreserved cell line Jurkat (Clone E6-1) from a -80°C freezer was thawed by gentle agitation of the vial in 20°C water. Directly after, the content in the vial was transferred to a 15 mL tube containing a 5 mL cell culture medium. The cells were centrifuged at 125 RCF for 5 min at 22 °C, followed by removal of the supernatant. Lastly, the cells were resuspended in a 10 mL cell culture medium, transferred to a 75 cm^3-flask, and an additional 20 mL cell culture medium was added.

3.2.3 Inducing Expression of PD-1

Jurkat cell cultures were subcultured in two 25 cm^3-flasks. The cells in one of the flasks were stimulated with 1 µg/mL PHA (Merck, Darmstad, Germany) and 50 ng/mL PMA (Merck, Darmstad, Germany) for 48 hours, as described by Yang et al. (2008) [74], while the cells in the other flask were kept unstimulated. After 48 hours, the cells were fixed by adding 1,6 % PFA (Thermo Fischer Scientific, Waltham, MA, USA) for 15 min with gentle agitation. The PFA was washed away, and the cells were incubated with heparin (Wockhardt, Mumbai, India) and FcR block reagent (Miltenyi Biotech, Bergisch Gladbach, Germany) for 15 min. The cells were then stained with 111Cd-CD3 [UCHT1], 145Nd-CD4 [RPA-T4], 157Gd-CD8a [HIT8a], and 166Er-anti-PD-1 [EH12.1] for 30 minutes in room temperature with shaking (1200 rpm). After this, the cells were again washed and then incubated with 1 mL of intercalation solution (containing 750 µL Maxpar® PBS (Fludigm, South San Fransisco, CA, USA), 250 µL 16 % PFA, 0,1 µM iridium (Fluidigm, South San Fransisco, CA, USA)) overnight at 4°C. The next day the samples were washed and run on CyTOF XT® (Fluidigm, South San Fransisco, CA, USA).

3.2 Healthy Donors

Peripheral blood samples from healthy donors were collected from the Blood Bank at Haukeland University Hospital (Bergen, Norway) according to agreement AIT60015 between Gjertsen lab and the Blood Bank. The healthy donors were males and females aged 18-70. All samples were collected in a BD vacutainer® EDTA tube with heparin (BD, Franklin Lakes, NJ, USA).

3.3 Patient Samples

Samples from 12 patients included in a basket study of three drugs was used in this thesis. Patients either received treatment with pembrolizumab (PD-1 inhibitor), atezolizumab (PD-L1 inhibitor) or lytix (immunotherapy drug). Peripheral blood from the patients was collected straight before (0 hours) and 2 hours after injection with the drug. This collection process was repeated for several treatment cycles, that took place every 3 weeks. Samples were immediately lysed and fixed after collection according to the approach described in section 3.5.1. Prior to the work in this thesis the samples had also been barcoded with palladium barcodes from Fluidigm (South San Fransisco, CA, USA) according to the approach described in section 3.5.2 and frozen at -80 °C. Table 3.5 gives an overview of the information about the patients and Figure 3.1 shows a swimmer plot with sample collections and response evaluations for each patient. The evaluation of response was conducted using RECIST (Response Evaluation Criteria in Solid Tumors). Some of the patients are missing the RECIST-evaluation due to

withdrawal from the trial or death before the first evaluation. An overview of the response evaluations is shown in Table 3.6. Clinical evaluation was used for the patients missing RECIST-evaluations if this was available. Any included clinical evaluation is marked with a star (*). All other evaluations were done by RECIST.

Table 3.5 Information about the patients included in this thesis. Includes patient-ID in the study, gender, age, diagnosis, treatment drug received, and total number of samples collected.

Patient information					
Patients	**Gender**	**Age**	**Diagnosis**	**Treatment**	**Number of samples**
Patient 10	Male	65	Penis cancer	Atezolizumab	8
Patient 11	Female	50	Ovarian cancer	Pembrolizumab	4
Patient 12	Female	73	Ovarian cancer	Pembrolizumab	4
Patient 13	Female	41	Small cell lung cancer (SCLC)	Pembrolizumab	11
Patient 14	Female	44	Cervix carcinoma	Pembrolizumab	9
Patient 15	Female	45	Anal cancer (squamous carcinoma)	Pembrolizumab	4
Patient 16	Male	76	Stomach cancer (adenocarcinoma)	Pembrolizumab	2
Patient 17	Female	60	Follicular thyroid carcinoma	Pembrolizumab	8
Patient 18	Female	69	Bile duct cancer (cholangiocarcinoma)	Pembrolizumab	2
Patient 19	Female	85	Vulvar cancer	Pembrolizumab	2
Patient 21	Female	70	Endometrial cancer	Pembrolizumab	2
Patient 22	Female	59	Triple negative breast cancer	Lytix	3

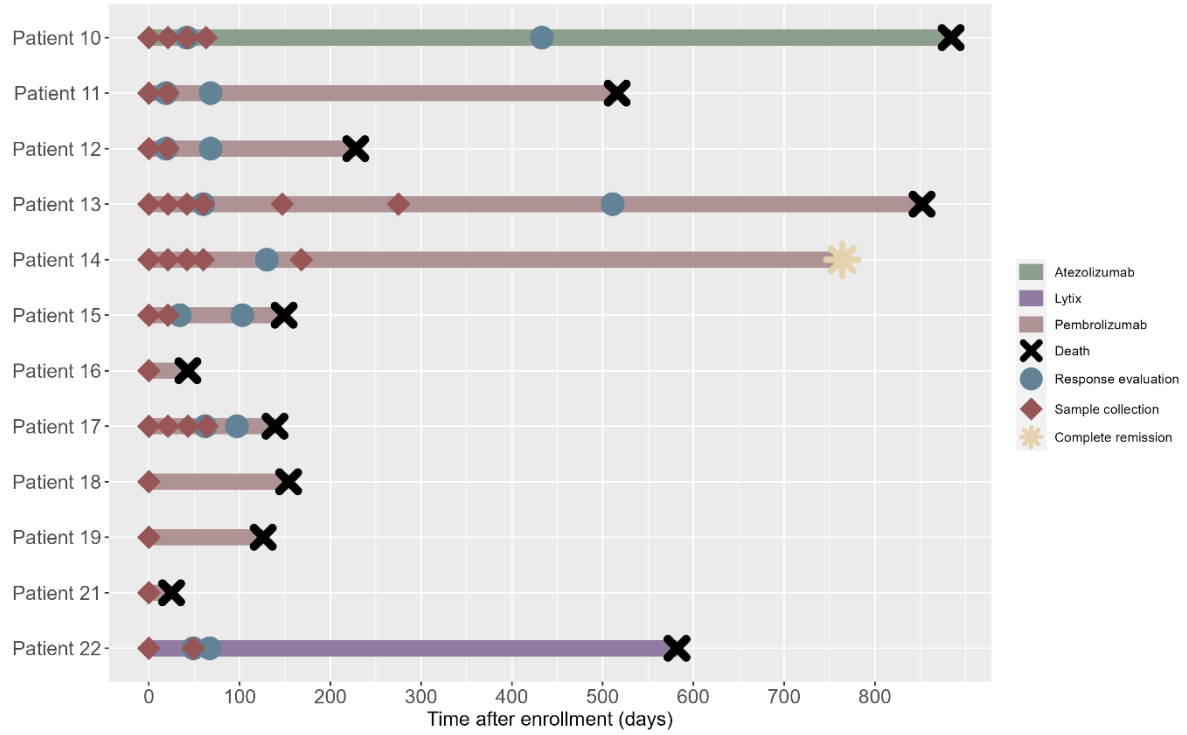

Figure 3.1 Overview of sample collection, clinical evaluations and time of death or complete remission for each patient. The colors of the lines indicate which treatment the patient received. Time is considered as days after enrollment.

Table 3.6 Overview of response evaluations and time of death for the patients. Most of the evaluations are RECIST-evaluations. The evaluations marker with a star (*) are clinical evaluations as RECIST-evaluations was not available for these patients. The date of the evaluation and time of death is counted as days after enrollment.

Response evaluations					
Patients	**First evaluation**	**Date first evaluation (days)**	**Last evaluation**	**Date last evaluation (days)**	**Time of death (days)**
Patient 10	Stable	42	Partial regression	433	884
Patient 11	Stable	67	Progressive	223	516
Patient 12	Progressive	19	Progressive	68	228
Patient 13	Partial regression	60	Progressive	511	852
Patient 14	Stable	130	Complete remission	764	-
Patient 15	Stable	34	Progressive	103	149
Patient 16	-	-	-	-	63
Patient 17	Progressive	62	Progressive	97	139
Patient 18	Stable*	64	Death*	154	154
Patient 19	-	-	Death*	126	126
Patient 21	-	-	Death*	-	25
Patient 22	Progressive	49	-	64	582

3.4 Pembrolizumab

Keytruda® (pembrolizumab) is produced by Merck (Darmstad, Germany). Leftover Keytruda® from patients receiving treatment at Haukeland University Hospital was kindly provided by PhD MPharm Ragnhild Haugse, Sjukehusapotekt i Bergen. Some pembrolizumab was conjugated using the same approach as described in section 3.1.2 with the Maxpar® X8 Polymer Labeling Kits.

3.5 Workflow of Experiments

The general workflow of the experiments conducted in this thesis is described in this section. The specifications and deviations from this workflow for each experiment are described in the sections further down.

3.5.1 Treatment and Fixation

Peripheral blood from a patient or healthy donor was collected for fixation. Some experiments using peripheral blood from healthy donors were treated with pembrolizumab in vitro before fixation. The remaining healthy and patient donor samples were directly fixed after collection. Samples were fixed by adding 1 mL peripheral blood to 12,5 mL BD Phosflow™ Lyse/Fix Buffer (BD, Franklin Lakes, NJ, USA) pre-diluted to 1x. The tube was inverted 8-10 times and incubated at 37 °C for 10 min. Then it was centrifuged at 500 RCF for 8 min at 4 °C and the supernatant was removed. The tube was then filled with 0,9 % NaCl solution (B. Braun, Melsungen, Germany), centrifuged again, and the supernatant was removed.

3.5.2 Barcoding

To enable the pooling of the samples before further processing, each sample was barcoded with a unique combination of metals that would identify the sample in the data analysis later. Either palladium or cisplatin isotopes were used for this purpose. Cells were first counted after the fixation, and then a maximum of 3 million cells from each sample were transferred to 2 mL Eppendorf tubes. The NaCl solution was removed by centrifuging the tubes at 800 RCF for 5 min and then discarding the supernatant. Each sample was resuspended in 1 mL of 1x Maxpar® Barcode Perm Buffer (Fluidigm, South San Francisco, CA, USA) and centrifuged again before removing the supernatant. The cells were then resuspended in 800 µL, for the cells to be barcoded with palladium using the Cell-ID™ 20-plex Barcoding Kit (Fluidigm, South San Francisco, CA, USA), or 100 µL, for the cells to be barcoded with cisplatin, of 1x Maxpar® Barcode Perm Buffer. The palladium barcodes (10 µL) were resuspended in 90 µL of 1x Maxpar® Barcode Perm Buffer and transferred to the respective samples. Then, the samples were incubated at room temperature for 30 min. 15 min into the incubation, the samples were gentle vortexed. 2 µL of the cisplatin barcodes were added directly to the sample and incubated for 30 min with shaking. After the incubation, the tubes were washed two times by filling the tubes with Maxpar® CSB (Fluidigm, South San Francisco, CA, USA), centrifuging at 800 RCF for 5 min, and then removing the supernatant. Lastly, the samples were resuspended in Maxpar® CSB, pooled together, aliquoted, and frozen.

3.5.3 Extracellular Staining

Frozen cells were thawed quickly in cold water and then put on ice. The cells were centrifuged at 800 RCF for 5 min at room temperature, followed by removal of the supernatant. The next

step was a 15 min incubation with Maxpar® CSB, heparin, and FcR block to a total volume of 50 µL. A mixture of all extracellular antibodies used in the respective experiment was prepared to a total volume of 50 µL. Then, the cells were incubated with the extracellular antibody mixture for 30 min at room temperature with shaking (1200 rpm). After this, the cells were washed three times to remove excess antibodies by filling the tube with Maxpar® CSB, centrifuging at 800 RCF for 5 min, and discarding the supernatant.

3.5.4 Permeabilization and Intracellular Staining

To enable intracellular staining, permeabilization of the cells was first necessary. After the extracellular staining, the pelleted cells from the last wash were initially cooled on ice for 10 min. Then, 1 mL of methanol (Merck, Darmstad, Germany), pre-cooled to -20 °C, was added quickly while vortexing to avoid aggregation of the cells. The cells were then again incubated on ice for 15 min. Samples were washed three times by filling the tube with Maxpar® CSB, centrifuging at 600 RCF for 5 min, and then removing the supernatant. The cells were again incubated for 15 min with a total volume of 50 µL consisting of Maxpar® CSB, heparin, and FcR block. The mixture of intracellular antibodies was prepared and transferred to the sample, followed by incubation for 30 min at room temperature with shaking (1200 rpm). Cells were again washed three times with Maxpar® CSB, then centrifuged, and the supernatant was removed. The final step of the staining process was an over-night incubation at 4 °C with 1 mL intercalation solution (containing 750 µL Maxpar® PBS, 250 µL 4% PFA, 0,1 µM iridium) to detect DNA-containing cells.

3.5.5 Acquisition on Mass Cytometer

The following day, the intercalation solution was washed away by filling the tube with Maxpar® CSB, centrifuging at 600 RCF for 5 min, and the supernatant was removed. Cells were then counted and transferred to flow tubes so that each tube contained a maximum of $2{,}8\times10^6$ cells. An additional wash with Maxpar® CSB, centrifugation at 600 RCF for 5 min and removal of supernatant was conducted. Afterward, two equivalent washes with Cell Acquisition Solution (CAS) Plus (Fluidigm, South San Fransisco, CA, USA) was carried out. In between the two washes, the cell suspension was flushed through the filter in the cap of the flow tube. The pelleted cells were brought to the mass cytometer for acquisition. The mass cytometer used in all the experiments in this thesis is a CyTOF XT® (Fludigm, South San Fransisco, CA, USA). Before the acquisition of the samples, the instrument was tuned using a Tuning Solution (Fluidigm, South San Fransisco, CA, USA). CAS Plus, and 10 % EQ™ Six Element Calibration Beads (Fluidigm, South San Fransisco, CA, USA) was added to the samples so that the concentration in each tube was $0{,}7\times10^6$ cells/mL. Acquired data was stored as an .FCS file to be further processed.

3.5.6 Normalization and Data Clean-up

The data was automatically normalized for signal variation in the instrument over time. This was done by the instrument's software using the EQ™ Six Element Calibration Beads with known concentrations of six different metals. The processed .FCS file was then uploaded to Cytobank.org for data clean-up. Herein, a method described by Bagwell et al. (2020) was used to remove unwanted events in the data [75]. Figure 3.2 shows the gating strategy that was used for data cleanup. Gating refers to the process in which an area (a gate) is selected, based on

knowledge of cell characteristics, to decide which cells should be analyzed further. First, beads were gated out. Then, the Gaussian parameters residual, center, offset, width, and event length were used to gate out more unwanted events. Lastly, the mass channels of ^{191}Ir and ^{193}Ir were used to gate out cells that did not contain DNA.

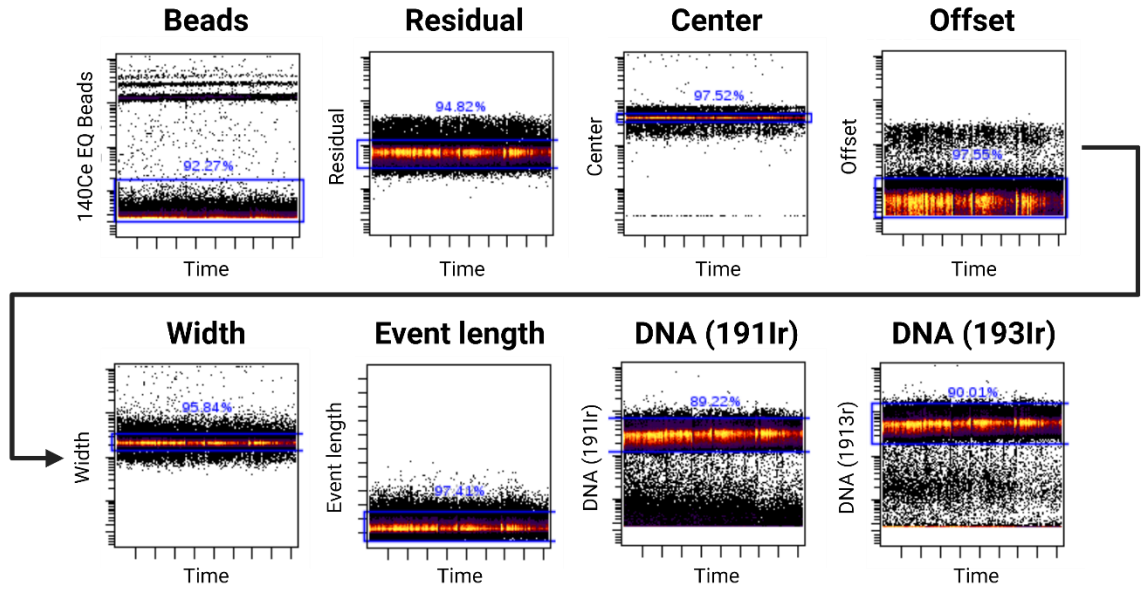

Figure 3.2 Gating strategy for data cleanup. The figure was adapted from [75].

3.5.7 Pre-Processing of Data

Normalized and cleaned-up data was further processed in RStudio (version 4.2.0) using the CATALYST package (1.20.1) [76]. If a barcode pool sample was split into several aliquots before data acquisition, the .FCS file from each aliquot needed to be concatenated. The next step was to debarcode all the data in this concatenated file to separate the data belonging to each initial sample before the pooling during the barcoding. This created one .FCS-file for each initial sample, enabling the data from each sample to be compared in later analysis. When working with mass cytometry data, isotope oxidation or signal overlap to adjacent channels, referred to as spillover, can occur. Therefore, the last pre-processing step was compensating the data using a previously generated spillover matrix.

3.5.8 Data Analysis and Gating

If necessary, the compensated files were uploaded to Cytobank.org, and T cells were gated using the strategy shown in Figure 3.3. Gated or ungated files were then further analyzed in RStudio (version 4.2.0). First, each dual count was arcsinh transformed with a cofactor of 5. Arcsinh transforming compresses the values of the high signal values while preserving the relative differences in the lower signal values. This enables small differences in the marker signals to be better visualized.

With the possibility of over 40 parameters per cell, mass cytometry data tends to be high dimensional. Thus, a dimensionality reduction is often necessary to make it easier to analyze

and visualize the data. Hence, FlowSOM, an unsupervised clustering algorithm, was used to create clusters of cells with similar expressions of markers [77]. Afterward, a dimensionality reduction algorithm, UMAP (Uniform Manifold Approximation and Projection), was used [78]. It visualized the low-dimensionality representation of the high-dimensional cluster data. Each dot in the UMAP is an event, corresponding to a single cell. Dots that are plotted close to each other have more similar expression profile, which makes it easier to identify clusters or groups of similar cells. A heatmap was generated, visualizing the median expression of a selection of markers for each cluster. The heatmap was used for immunophenotyping of the clusters using the markers shown in Table 3.5. The clusters were then merged or removed based on the immunophenotyping.

Arcsinh transformation of the data is beneficial to use in clustering and dimensionality reduction, but for calculating receptor occupancy it is important to keep the linearity in the data. Therefore, the dual count was used for the remaining data analysis and calculation of receptor occupancy. The 75th percentile dual count for each marker in each cluster was calculated, and the data was plotted as using the ggplot2 package [79].

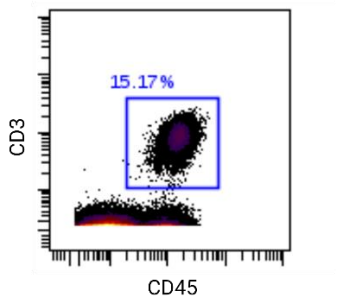

Figure 3.3 Gating strategy for T cells. Cells that were CD45^{+} and CD3^{+} was manually gated in Cytobank®.

Table 3.5 Overview of markers used for immunophenotyping.

Immunophenotyping	
Granulocytes	
Neutrophils	$CD45^-$ $CD66b^+$
Monocytes	$CD45^+$ $CD11c^+$ $CD14^+$/ $CD16^+$
Dendritic cells	
mDC	$CD45^+$ HLA-DR^+ $CD11c^+$
pDC	$CD45^+$ $CD123^+$
Natural killer cells	
NK cells	$CD45^+$ $CD56^+$
NKT cells	$CD45^+$ $CD3^+$ $CD56^+$
B-cells	$CD45^+$ $CD20^+$
T cells	
Helper (Th)	$CD45^+$ $CD3^+$ $CD4^+$
Cytotoxic (Tc)	$CD45^+$ $CD3^+$ $CD8^+$
Double-positive (Tdp)	$CD45^+$ $CD3^+$ $CD4^+$ $CD8^+$
Double-negative (Tdn)	$CD45^+$ $CD3^+$ CD4- $CD8^-$
Naïve (T_N)	$CD45^+$ $CD3^+$ $CD4^+$/$CD8^+$ $CD45RA^+$ $CD27^+$
Central memory (T^{CM})	$CD45^+$ $CD3^+$ $CD4^+$/$CD8^+$ $CD45RA^-$ $CD27^+$
Effector memory (T_{EM})	$CD45^+$ $CD3^+$ $CD4^+$/$CD8^+$ $CD45RA^-$ $CD27^-$
Terminally differentiated effector memory (T_{EMRA})	$CD45^+$ $CD3^+$ $CD4^+$/$CD8^+$ $CD45RA^+$ $CD27^-$
Activated T cells ($T_{act.}$)	$CD45^+$ $CD3^+$ $CD4^+$/$CD8^+$ $CD25^+$

3.6 Experiments

This section contains a description of the experiments conducted in this thesis. Any deviations from the general workflow described in the previous section or specifications for the experiment are described for each experiment.

3.6.1 Saturation of Pembrolizumab on Cell Surface Receptor PD-1

An experiment was conducted to check at which concentration pembrolizumab reaches saturation on PD-1 in healthy donors. Peripheral blood from three healthy donors was collected. 1 mL of peripheral blood from the three healthy donors was fixed immediately. The remaining blood was transferred in 1 mL aliquots to a 24-well plate and incubated with increasing concentration of 159Tb-pembrolizumab: 0; 0,01; 0,1; 1; 10 µg/mL in a humidified incubator at 37°C with 5% CO_2 for 30 min. The samples were immediately fixed after incubation and then barcoded. The cells were stained with the extracellular panel, followed by permeabilization, and staining with the intracellular panel. Cells were run on CyTOF XT®, and data processing and analysis were done as described above. Cells were not gated to check for populations that did not bind 159Tb-pembrolizumab.

3.6.2 Comparison of PD-1 Antibody Clones in Healthy Donors

Three PD-1 antibodies were acquired and in-house conjugated for being tested as competing antibodies that could detect receptors not bound by pembrolizumab: 166Er-anti-PD-1 [EH12.1], 176Yb-anti-PD-1[EH12.2H7], and 168Er-anti-PD-1 [MIH4]. Initially, we wanted to

check the how the signal of the three PD-1 clones was compared to that of 159Tb-pembrolizumab in healthy donor blood before fixation. Peripheral blood from three healthy donors was collected. The blood from each of the healthy donors was separately incubated with 2,5 µg/mL of 159Tb-pembrolizumab, 166Er-anti-PD-1 [EH12.1], 176Yb-anti-PD-1[EH12.2H7] or 168Er-anti-PD-1 [MIH4] in a humidified incubator at 37°C with 5% CO_2 for 30 min. Following the incubation, the samples were fixed, barcoded and stained with a backbone panel of the most important immunophenotyping markers. Cells were not permeabilized and stained with an intracellular panel but incubated with the intercalation solution. The samples were run on CyTOF XT®. The data was not gated but processed and analyzed according to the workflow described in section 3.5.

3.6.3 Competition Assay

To decide which PD-1 clone was the most fit to detect PD-1 receptors not blocked by pembrolizumab, it was necessary to perform a competition assay to determine which clones (EH12.1, EH12.2H7, MIH4) were competing against pembrolizumab. In this experiment, peripheral blood from three healthy donors was treated with 0 µg/mL, 25 µg/mL unconjugated pembrolizumab, or 25 µg/mL 159Tb-pembrolizumab. Samples were incubated for 15 min or 2 hours in a humidified incubator at 37°C with 5% CO_2. Then, the cells were fixed and barcoded. During the extracellular staining, the cells were stained with increasing concentrations of the three anti-PD-1 clones (0; 0,4; 2; 10 µg/mL). Each clone was stained in separate tubes for each concentration. 173Yb-anti-IgG4 [HP6025] was not included in the panel for this extracellular staining. All samples were permeabilized and stained with the intracellular panel before being run on CyTOF XT®. The data was not gated but processed and analyzed as previously described.

3.6.4 Titration of 166Er-anti-PD-1 [EH12.1]

166Er-anti-PD-1 [EH12.1] was titrated to decide which dilution to use in the panel. Peripheral blood from three healthy donors was fixed immediately after collection. Samples were barcoded and titrated as described in section 3.1.3. 166Er-anti-PD-1 [EH12.1] was serial diluted to a concentration of 0; 0,16; 0,8; 4; 20 µg/mL. No permeabilization or intracellular staining was conducted, but the cells were incubated with an intercalation solution. Samples were run on CyTOF XT® and analyzed without gating.

3.6.5 Titration of 173Yb-anti-IgG4 [HP6025]

173Yb-anti-IgG4 [HP6025] was intended to be used as a secondary antibody to detect bound pembrolizumab. Therefore, it needed to be titrated on samples saturated with pembrolizumab to decide which dilution to use in the panel. Peripheral blood from three healthy donors was collected and transferred to 1 mL aliquots in a 24-well plate. 1 mL of blood from each donor was fixed immediately. The blood in the 24-well plate was treated with increasing concentrations of pembrolizumab (0; 0,01; 0,1; 1; 10; 100 µg/mL) and incubated in a humidified incubator at 37°C with 5% CO_2 for 30 min. Cells were then fixed and barcoded. The titration was done as described in section 3.1.3 with a serial dilution of 173Yb-anti-IgG4 [HP6025] of 0,625; 1,25; 2,5; 5; 10 µg/mL, corresponding to a dilution of 1:800, 1:400, 1:200, 1:100 and 1:50 in the antibody panel. This titration had no permeabilization or intracellular

staining, but cells were incubated with an intercalation solution. The samples were run on CyTOF XT® and analyzed without gating.

3.6.6 Receptor Occupancy in Patient Samples

The assay was tested on samples from 12 patients receiving treatment with pembrolizumab, atezolizumab or lytix and a mixture of cells from peripheral blood of 4 healthy donors. An overview of the patients and collected samples can be found in section 3.3. All samples had already been fixed, barcoded, and frozen prior to the work of this thesis. The cells were thawed in cold water before being stained with the extracellular panel, permeabilized, and then stained with the intracellular panel. Samples were incubated with intercalation solution and run on CyTOF XT®. The data underwent normalization, data clean-up, and pre-processing as described in section 3.5.6 and 3.5.7.

Due to the large amount of data generated, subsamples of the dataset were used in the data analysis. First, a subsample of 10000 cell events per timepoint for each patient was taken out and clustered as described in section 3.5.8. The purpose of this was to investigate the signal of 166Er-anti-PD-1 [EH12.1] and 173Yb-anti-IgG4 [HP6025] in all cell populations. For the calculation of receptor occupancy, T cells were initially gated in Cytobank.org as shown in Figure 3.3, and this subpopulation was further analyzed as described in section 3.5.8.

The receptor occupancy was determined using two different approaches. The first approach was based on a free receptor assay, using the competing labeled antibody 166Er-anti-PD-1 [EH12.1]. The first sample in the first treatment cycle for each patient was taken before any injection of drug. Assuming 166Er-anti-PD-1 [EH12.1] was used in saturating amounts, it should detect all available PD-1 receptors, corresponding to 100 % free receptors. Thus, the dual count of the consecutive samples divided by the dual count of the first sample would provide a receptor occupancy.

The second approach used an 173Yb-anti-IgG4 [HP6025] antibody to measure bound pembrolizumab on each cell. In the first sample of all the patients, there should not be detected any pembrolizumab by the 173Yb-anti-IgG4 [HP6025] antibody. Therefore, the dual count of the first sample was subtracted from each of the consecutive samples. Since the maximal amount of bound pembrolizumab is unknown, the dual counts of all the samples were divided by the dual count of the first sample to get a relative change in receptor occupancy. Therefore, it is important to be aware of that the bound receptor approach displays a relative change in receptor occupancy rather than an absolute receptor occupancy. The equations used for the calculations is shown in Equation 1 and 2, and the principle of the receptor occupancy approach in this thesis is shown in Figure 3.4.

Equation 1. Receptor occupancy by free receptor approach using 166Er-anti-PD-1 [EH12.1].

$$RO = \frac{s_x}{s_0} \cdot 100\%$$

Equation 2. Receptor occupancy by bound receptor approach using 173Yb-anti-IgG4 [HP6025].

$$RO = \left(\frac{s_x}{s_0} - 1\right) \cdot 100\%$$

RO = receptor occupancy

s_0= signal (dual count) of first sample

s_x= signal (dual count) of a consecutive sample

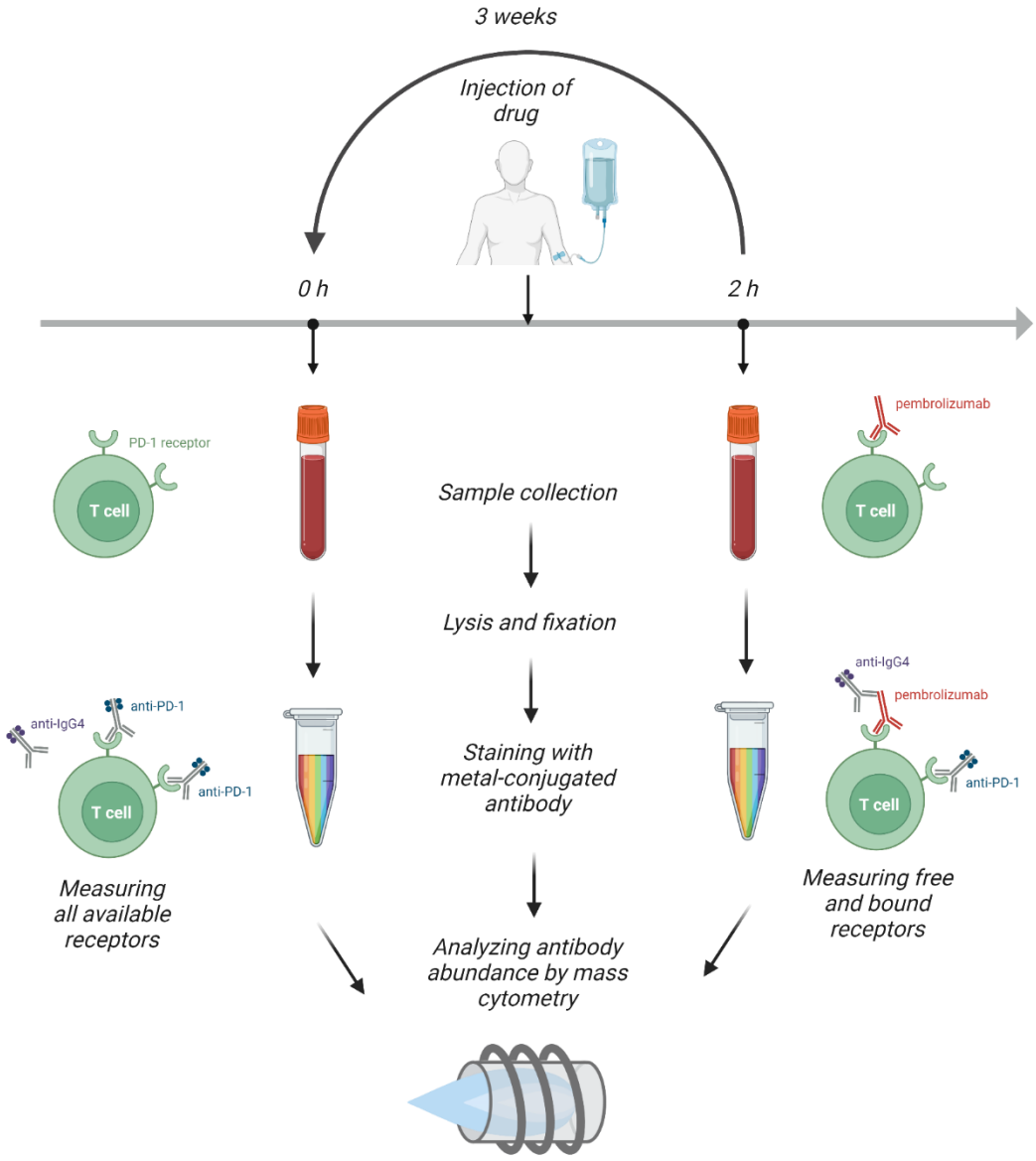

Figure 3.4 Principle of the receptor occupancy approach used on the patient samples. Blood collected at 0 h and 2 hours after injection for each treatment cycle (every 3 weeks) is lysed, fixed and stained with metal-conjugated antibodies, including 166Er-anti-PD-1 [EH12.1] and 173Yb-anti-IgG4 [HP6025]. The abundance of the antibodies in each sample is measured as dual counts by mass cytometry. In the sample collected before injection, 166Er-anti-PD-1 [EH12.1] detects all available PD-1 receptors while 173Yb-anti-IgG4 [HP6025] should not detect any pembrolizumab. In all the samples collected after injection, 166Er-anti-PD-1 [EH12.1] detects free receptors that are not occupied by pembrolizumab and 173Yb-anti-IgG4 [HP6025] measures bound pembrolizumab.

3.7 Quantum™ Simply Cellular Beads®

The use of Quantum™ Simply Cellular® (QSC) Beads was tested for the purpose of standardization across mass channels in mass cytometry and the quantification of Antibodies Bound per Cell (ABC). The Quantum™ Simply Cellular® anti-Mouse for mouse mAbs (Bangs Laboratories, Fishers, IN, USA) , kindly provided by PhD Sonia Gavasso, consist of 5 bottles, 1 blank and 4 populations that can bind increasing amounts of antibodies. The QSC beads are intended to be used in flow cytometry. Therefore, the protocol from Bangs Laboratories was adapted for being used in mass cytometry in this thesis.

First, the bottles were manually shaken to ensure a uniform suspension of the microspheres. The blank population was kept unstained. The other populations were stained separately by adding a drop of the QSC beads, 50 µl CSB and 1 µl of 166Er-anti-PD-1 [EH12.1] to an Eppendorf tube and gently flicking the tube. The beads were washed twice by adding 1 mL CSB to the tubes, centrifuging at 2500 RCF and removing the supernatant. Following this, the beads were transferred to a flow tube and washed like the previous washes, using CAS Plus instead of CSB. The beads were resuspended in CAS Plus before being run on CyTOF XT®, without the addition of EQ™ Six Element Calibration Beads.

3.8 Statistical Analysis

A preliminary statistical analysis was performed to exemplify an approach for investigating receptor occupancy as a predictive biomarker. The aim of this preliminary statistical analysis was to check if there was a significant difference in the mean dual count or the mean receptor occupancy of patients responding to treatment versus those that did not. For this purpose, the patients having received treatment with pembrolizumab was categorized as a responder or a non-responder according to Table 3.7. The categorization was conducted based on the best evaluation the patient had. A responder was considered to have complete remission, partial regression, or stable disease. A non-responder was defined as patients with progressive disease or a patient that died. Patient 16 was excluded from the analysis as this patient neither had a RECIST-evaluation, nor a clinical evaluation. Due to the lack of longitudinal sample collection for most of the patients, only the sample 2 hours after the first injection was used for the statistical analysis.

Table 3.7 Response categorization of patients having received treatment with pembrolizumab. All evaluations are RECIST-evaluations, except for the ones marked with a start (*). These are clinical evaluations due to RECIST-evaluations nor being available for these patients. Patients were categorized based on their best evaluation. Complete remission, partial regression and stable disease corresponded to a responder, while progressive disease or death corresponded to a non-responder.

Response categorization		
Patient-ID	**Best evaluation**	**Response category**
Patient 11	Stable	Responder
Patient 12	Progressive	Non-responder
Patient 13	Partial regression	Responder
Patient 14	Complete remission	Responder
Patient 15	Stable	Responder
Patient 16	-	Excluded
Patient 17	Progressive	Non-responder
Patient 18	Stable*	Responder
Patient 19	Death*	Non-responder
Patient 21	Death*	Non-responder

A t-test was used to determine if there was any significant difference in the mean dual count or receptor occupancy of the responders and non-responders. This was conducted for the dual count of 166Er-anti-PD-1 [EH12.1], the dual count of 173Yb-anti-IgG4 [HP6025], the receptor occupancy of 166Er-anti-PD-1 [EH12.1], and the receptor occupancy of 173Yb-anti-IgG4 [HP6025] for three cell subsets: cytotoxic T cells (central memory), helper T cells (central memory), and activated helper T cells (central memory). First, a two-sided F-test was conducted to check if the variance between responders and non-responder were equal or not. The null hypothesis of this test is that the variance is equal. Thus, a p-value lower than 0,05 would reject the null hypothesis, that is, we would assume that the variance is unequal. In this case, two-sided unequal variance t-test was used. If the variance was assumed to be equal, two-sided equal variance t-test was used. Both t-tests were conducted as two-sample t-tests and RStudio (version 4.2.0) was used to generate the p-values. The null hypothesis of both t-tests is that the difference in mean for responders and non-responders are 0. That means that if the p-value is higher than 0,05, there is no significant difference in the mean of the two patient groups. Correspondingly, if the p-value is lower than 0,05, there is a significant difference in the mean of responders and non-responders.

4 Results

4.1 Development of Panel

4.1.1 Saturation of Pembrolizumab on Cell Surface Receptor PD-1

A saturation experiment was conducted to assess at which concentrations treatment with pembrolizumab saturated available PD-1 receptors on cells in healthy donor peripheral blood. For this purpose, pembrolizumab was conjugated with 159Tb isotopes (159Tb-pembrolizumab) to enable the direct quantification of 159Tb-pembrolizumab bound PD-1 receptors. Increasing concentrations of 159Tb-pembrolizumab were used (0; 0,01; 0,1; 1; 10 µg/mL) to treat healthy donor peripheral blood (n=3). Samples were analyzed as described in section 3.6.1. Figures 4.2 a) and b) show the UMAP and heatmap from the data analysis.

Figure 4.2 c), colored by the scaled 159Tb-pembrolizumab dual count, and Figure 4.2 d), displaying the signal of 159Tb-pembrolizumab with increasing concentrations, show that 159Tb pembrolizumab binds specifically to T cells. Especially memory T cells seems to have increased 159Tb-pembrolizumab bound PD-1 compared to the naïve cells for all three donors. The signal of 159Tb-pembrolizumab flattens out around 1 µg/mL for all the T cell subsets, suggesting a saturation level of 159Tb-pembrolizumab at approximately 1 µg/mL in healthy donors. There is an increase in the signal of 159Tb-pembrolizumab in neutrophils at 10 µg/mL.

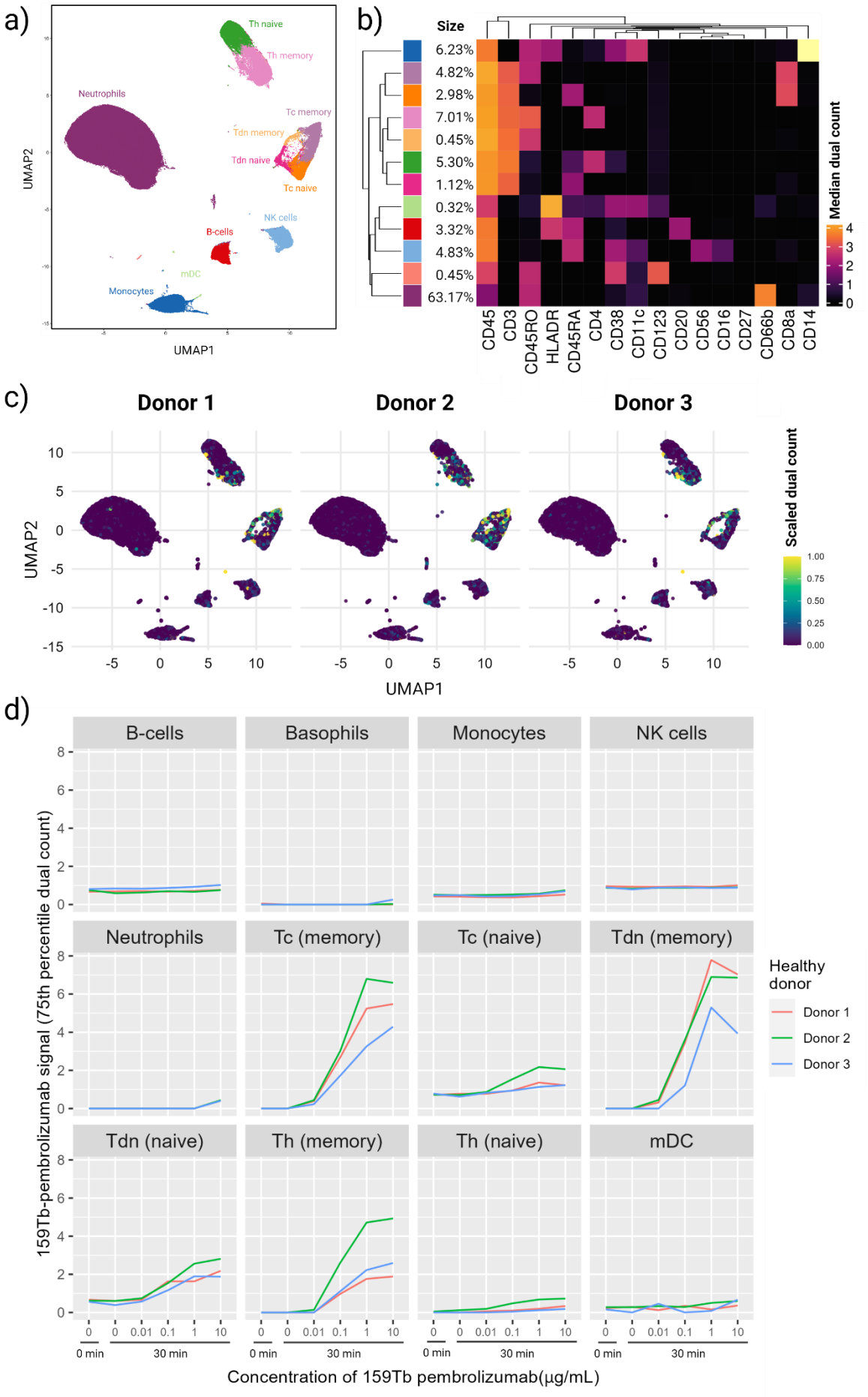
a)
Th naive
Th memory
Neutrophils
Tc memory
Tdn memory
Tdn naive
Tc naive
NK cells
B-cells
mDC
Monocytes
UMAP2
UMAP1
b)
Size
6.23%
4.82%
2.98%
7.01%
0.45%
5.30%
1.12%
0.32%
3.32%
4.83%
0.45%
63.17%
CD45
CD3
CD45RO
HLADR
CD45RA
CD4
CD38
CD11c
CD123
CD20
CD56
CD16
CD27
CD66b
CD8a
CD14
Median dual count
c)
Donor 1
Donor 2
Donor 3
UMAP2
UMAP1
Scaled dual count
d)
B-cells
Basophils
Monocytes
NK cells
Neutrophils
Tc (memory)
Tc (naive)
Tdn (memory)
Tdn (naive)
Th (memory)
Th (naive)
mDC
159Tb-pembrolizumab signal (75th percentile dual count)
0 min
30 min
Concentration of 159Tb pembrolizumab(µg/mL)
Healthy donor
Donor 1
Donor 2
Donor 3

Figure 4.2 Results from immunophenotyping and saturation of 159Tb-pembrolizumab. a) UMAP showing assigned cell populations from clustering and immunophenotyping. b) Heatmap showing median dual count of markers used for immunophenotyping. c) UMAP for each of the healthy donors showing scaled dual count of 159Tb-pembrolizumab. d) 159Tb-pembrolizumab signal for all cell clusters, revealing binding to T cells (especially on memory T cells) and saturation around 1 µg/mL.

4.1.2 Comparison of PD-1 Antibody Clones in Healthy Donors

To determine which PD-1 antibody clone could be used for detecting receptors not bound by pembrolizumab in the receptor occupancy assay, an assessment of their staining patterns and signals compared to that of 159Tb-pembrolizumab was considered useful. Peripheral blood from healthy donors (n=3) was incubated separately with 2,5 µg/mL (a concentration that was a bit above the saturation level of 159Tb-pembrolizumab) of three PD-1 antibody clones (EH12.1, EH12.2H7 MIH4) and 159Tb-pembrolizumab. Samples were analyzed as described in section 3.6.2, and the results are shown in Figure 4.3. The cells were phenotyped as shown in the UMAP in Figure 4.3 a). Figure 4.3 b) shows the median dual count of the markers used for immunophenotyping for each of the clusters.

Figure 4.3 c) shows the anti-PD-1 signal measured for each cell population for all three donors. Generally, 166Er-anti-PD-1 [EH12.1] seems bind the best, producing the highest signals, followed by 159Tb-pembrolizumab, 176Yb-anti-PD-1 [EH12.2H7], and, lastly, 168Er-anti-PD-1 [MIH4]. The relative difference in the signal between each of the three clones and 159Tb-pembrolizumab seems to follow the same pattern for all the donors in almost all cell populations. From Figure 4.3 c) and d), it seems that the binding of the four antibodies is specific for T cells, consistent with the binding observed in the saturation experiment described above in section 4.1.1. From these results, 166Er-anti-PD-1 [EH12.1] appears to have the highest affinity. Preferably, an antibody with similar affinity as the drug itself should be used in a free receptor assay as this does not over- or underestimate the number of available receptors. Therefore, 166Er-anti-PD-1 [EH12.1], producing a stronger signal, or 176Yb-anti-PD-1 [EH12.2H7], with a slightly weaker signal, would be the best candidates for the free receptor approach.

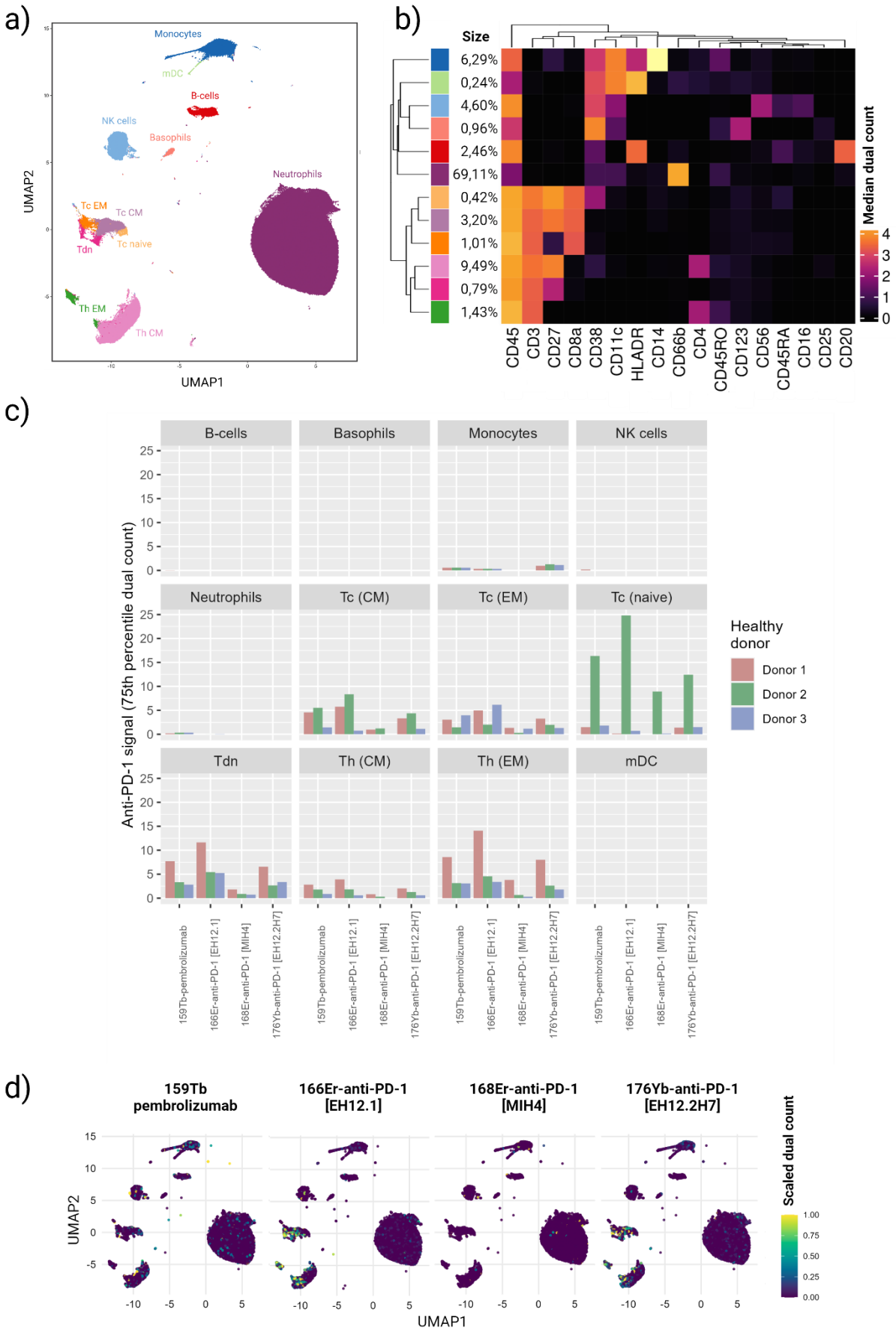
a)
Monocytes
mDC
B-cells
NK cells
Basophils
Neutrophils
Tc EM
Tc CM
Tdn
Tc naive
Th EM
Th CM
UMAP2
UMAP1
b)
Size
6,29%
0,24%
4,60%
0,96%
2,46%
69,11%
0,42%
3,20%
1,01%
9,49%
0,79%
1,43%
CD45
CD3
CD27
CD8a
CD38
CD11c
HLADR
CD14
CD66b
CD4
CD45RO
CD123
CD56
CD45RA
CD16
CD25
CD20
Median dual count
c)
B-cells
Basophils
Monocytes
NK cells
Neutrophils
Tc (CM)
Tc (EM)
Tc (naive)
Tdn
Th (CM)
Th (EM)
mDC
Anti-PD-1 signal (75th percentile dual count)
159Tb-pembrolizumab
166Er-anti-PD-1 [EH12.1]
168Er-anti-PD-1 [MIH4]
176Yb-anti-PD-1 [EH12.2H7]
Healthy donor
Donor 1
Donor 2
Donor 3
d)
159Tb pembrolizumab
166Er-anti-PD-1 [EH12.1]
168Er-anti-PD-1 [MIH4]
176Yb-anti-PD-1 [EH12.2H7]
UMAP2
UMAP1
Scaled dual count

Figure 4.3 Results from comparison of the three PD-1 clones (166Er-anti-PD-1 [EH12.1], 176Yb-anti-PD-1 [EH12.2H7], and 168Er-anti-PD-1 [MIH4]) and 159Tb-pembrolizumab. a) UMAP showing assigned cell populations from clustering and immunophenotyping. b) Heatmap from showing clusters and markers used for immunophenotyping. c) Barplot of the signal of each antibody in each healthy donor. 166Er-anti-PD-1 [EH12.1] has the highest signal, followed by 159Tb-pembrolizumab, 176Yb-anti-PD-1 [EH12.2H7], and 168Er-anti-PD-1 [MIH4]. d) UMAP exemplified for donor 1 showing scaled signal of each of the antibodies.

4.1.3 Competition assay

To measure free receptors, it is necessary that the PD-1 antibody clone used competes against pembrolizumab for binding to the PD-1 receptor. Therefore, a competition assay was conducted to decide which of the three antibody clones (EH.12.1, EH.12.2H7 and MIH4) were competing and, if so, if the incubation time or conjugation of 159Tb to pembrolizumab affected the competition. The blood from the healthy donors (n=3) was incubated with either conjugated, unconjugated pembrolizumab, or nothing for either 15 or 120 min. After fixation, each of the three antibody clones were added in increasing concentrations (0; 0,4; 2; 10 µg/mL) in separate tubes, and the samples were analyzed as described in section 3.6.3. The results are shown in Figure 4.4.

To investigate the effect of incubation time, the 159Tb-pembrolizumab signal in samples incubated for 15 or 120 minutes and stained with increasing concentrations of the clone EH12.1 were compared. From Figure 4.3 a), one can see that the 159Tb-pembrolizumab signal after 120 min samples (solid line) is consistently higher than in the 15 min samples (dashed line) for almost all T cell populations. With the exception of smaller cell populations (e.g. Tdn), no clear reduction in 159Tb-pembrolizumab was observed with increasing EH12.1 staining, suggesting that this antibody clone was not able to displace PD-1 bound 159Tb-pembrolizumab.

Whether the conjugation of pembrolizumab affected the competition was of interest as well. Therefore, the binding of PD-1 by 166Er-anti-PD-1 [EH12.1] at different concentrations was compared in samples that were incubated with conjugated and unconjugated pembrolizumab before fixation of the cells (Figure 4.3 b). We observed that the binding of PD-1 by 166Er-anti-PD-1 [EH12.1] in the samples treated with 159Tb-pembrolizumab is higher than that of unconjugated pembrolizumab. This implies that 166Er-anti-PD-1 [EH12.1] experiences more competition in the samples treated with unconjugated pembrolizumab and that more 166Er-anti-PD-1 [EH12.1] can bind to PD-1 in the samples treated with 159Tb-pembrolizumab.

Based on the finding with incubation time and conjugation, a sample incubated with unconjugated pembrolizumab for 120 min before fixation was chosen to investigate the competition of the three clones individually against pembrolizumab. The results are shown in Figure 4.3 c). A change between signal in samples that were not treated (solid line) and the samples treated with pembrolizumab (dashed line) will suggest a competition. For 168Er-anti-PD-1 [MIH4], there is low or almost no change between the samples with or without pembrolizumab, suggesting that this clone is not competing for the PD-1 receptor or that the clone does not work on fixed cells. Both 166Er-anti-PD-1 [EH12.1] and 176Yb-anti-PD-1

[EH12.2H7] seems compete against pembrolizumab with quite similar decreases in PD-1 binding from untreated to treated samples. Both clones also seem to be saturated when stained in fixed cells at around 2 µg/mL. Since the results from this experiment suggested that unconjugated pembrolizumab might have higher affinity than the conjugated one, it is likely that 166Er-anti-PD-1 [EH12.1] is the anti-PD-1 antibody that has the most similar affinity, as it showed a bit higher expression than 159Tb pembrolizumab in Figure 4.3. Combined with other preliminary findings, 166Er-anti-PD-1 [EH12.1] was chosen as the antibody to detect free receptors in the receptor occupancy assay.

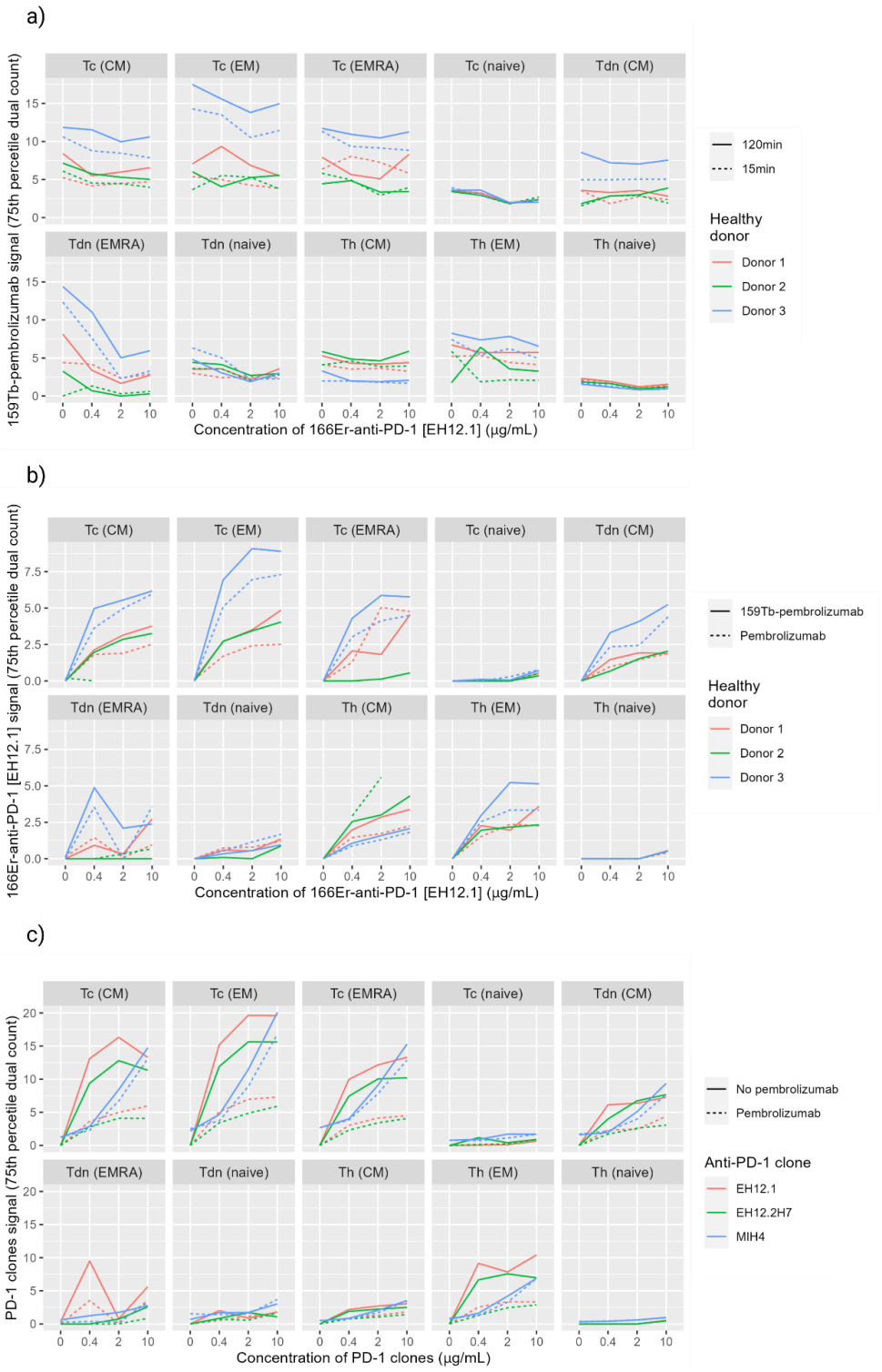

Figure 4.3 Results from the competition experiment. a) Comparing signal of 159Tb-pembrolizumab for samples incubated for 15 min and 120 min before fixation to assess the effect of incubation time. The samples were stained with increasing concentrations of 166Er-anti-PD-1 [EH12.1]. b) Comparing signal of 166Er-anti-PD-1 [EH12.1] for samples incubated with 159Tb-pembrolizumab or unconjugated pembrolizumab before fixation to assess the effect of conjugation. After fixation, samples were stained with increasing concentrations of 166Er-anti-PD-1 [EH12.1]. c) Comparing change in signal for each of the three PD-1 clones (166Er-anti-PD-1 [EH12.], 176Yb-anti-PD-1 [EH12.2H7], and 168Er-anti-PD-1 [MIH4]) between sample with and without pembrolizumab. Samples were stained with increasing concentrations of the respective clone.

4.1.4 Titration of 166Er-anti-PD-1 [EH12.1]

A titration was conducted to decide which concentration level of 166Er-anti-PD-1 [EH12.1] was to be used in the assay, corresponding to the dilution of the antibody in the panel. Fixed cells from healthy donors (n=3) were stained with increasing concentrations of 166Er-anti-PD-1 [EH12.1] (0; 0,16; 0,8; 4; 20 µg/mL). The results of the titrations are displayed in Figure 4.4. 166Er-anti-PD-1 [EH12.1] seems to reach saturation around 0,8-4 µg/mL for most of the T cell populations. Indications of unspecific binding can be observed at 20 µg/mL, where the signal of 166Er-anti-PD-1 [EH12.1] is increasing in cell populations that are not expected to express PD-1. For neutrophils, the unspecific binding is already visible at 4 µg/mL. From the results shown in Figure 4.3 c) in the previous section, it seems that the sample that received no treatment with pembrolizumab (solid line) reached saturation of 166Er-anti-PD-1 [EH12.1] at a concentration of 2 µg/mL. Consequently, the concentration of 166Er-anti-PD-1 [EH12.1] in the receptor occupancy assay was decided to be 2,5 µg/mL, corresponding to a dilution of 1:200 in the panel. The rationale for this was that it was desirable to choose a concentration that was a bit above the known level of saturation of 166Er-anti-PD-1 [EH12.1] and, at the same time, avoid as much unspecific staining as possible in neutrophils and other populations expected to be PD-1 negative.

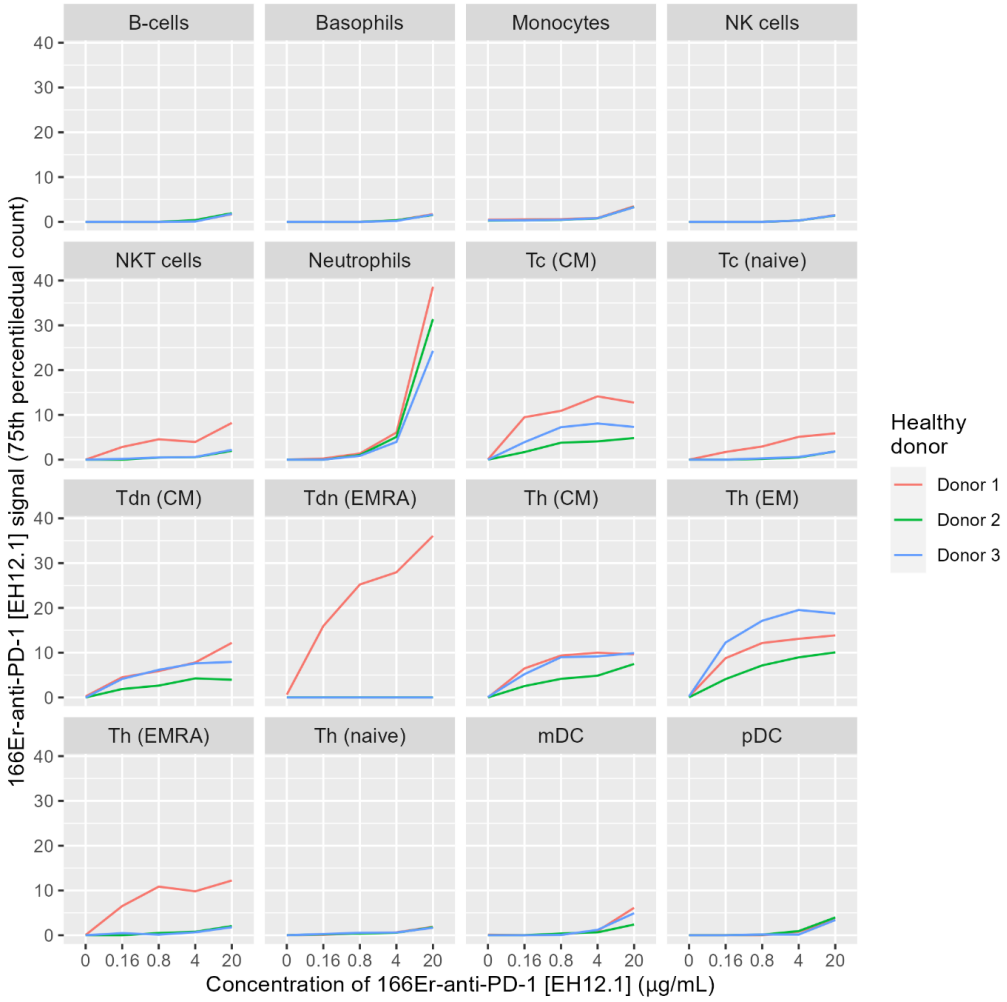

Figure 4.4 Titration of 166Er-anti-PD-1 [EH12.1]. T cells seem to be saturated around 0,8-4 µg/mL. Cell populations expected to be negative for PD-1 seem to express unspecific binding at 20 µg/mL, except for neutrophils that already show signs of unspecific binding at 4 µg/mL.

4.1.5 Titration of 173Yb-anti-IgG4 [HP6025]

As pembrolizumab is an IgG4 antibody, one approach to detect PD-1 bound pembrolizumab is to target it using a secondary IgG4 antibody. We, therefore, titrated 173Yb-anti-IgG4 [HP6025] on healthy donor blood (n=3) that, before fixation, was incubated with increasing concentrations of pembrolizumab (0; 0,01; 0,1; 1; 10; 100 µg/mL). After the incubation, the samples were fixed and stained with increasing concentrations of 173Yb-anti-IgG4 [HP6025] (0,625; 1,25; 2,5; 5; 10 µg/mL). Figure 4.5 shows the results from the titration.

Figure 4.5 a) shows a UMAP of the assigned clusters and Figure 4.5 b) shows the heatmap with the scaled dual counts for the markers used in immunophenotyping. From Figure 4.5 c) we notice that 173Yb-anti-IgG4 [HP6025] does not seem to be specific for the populations expected to bind pembrolizumab. The results in Figure 4.2 d) show that the binding of 159Tb-pembrolizumab is mainly on T cells, while 173Yb-anti-IgG4 [HP6025] in Figure 4.5 c) seems to bind to other cells as well. There seems to be increased signal of 173Yb-anti-IgG4 [HP6025] for increasing concentration of pembrolizumab for the highest staining concentration of 173Yb-

anti-IgG4 [HP6025] (10 µg/mL) in some of the T cell populations. Nevertheless, the signal is also high at this concentration level for many populations expected to not express PD-1. The increase in the lower staining concentrations of 173Yb-anti-IgG4 [HP6025] is not as visible as for the one at 10 µg/mL.

173Yb-anti-IgG4[HP6025] does not seem to be as specific for detecting pembrolizumab in healthy donors. Despite this, the antibody was still included in the panel to be tested on the patient samples. 10 µg/mL, corresponding to a dilution of 1:50 in the panel, was the only concentration level that showed a noticeable increase in signal intensity of 173Yb-anti-IgG4[HP6025] with increasing concentration of pembrolizumab. Therefore, this concentration was chosen, even though signal on other cell populations was expected to be present in the patient samples as well.

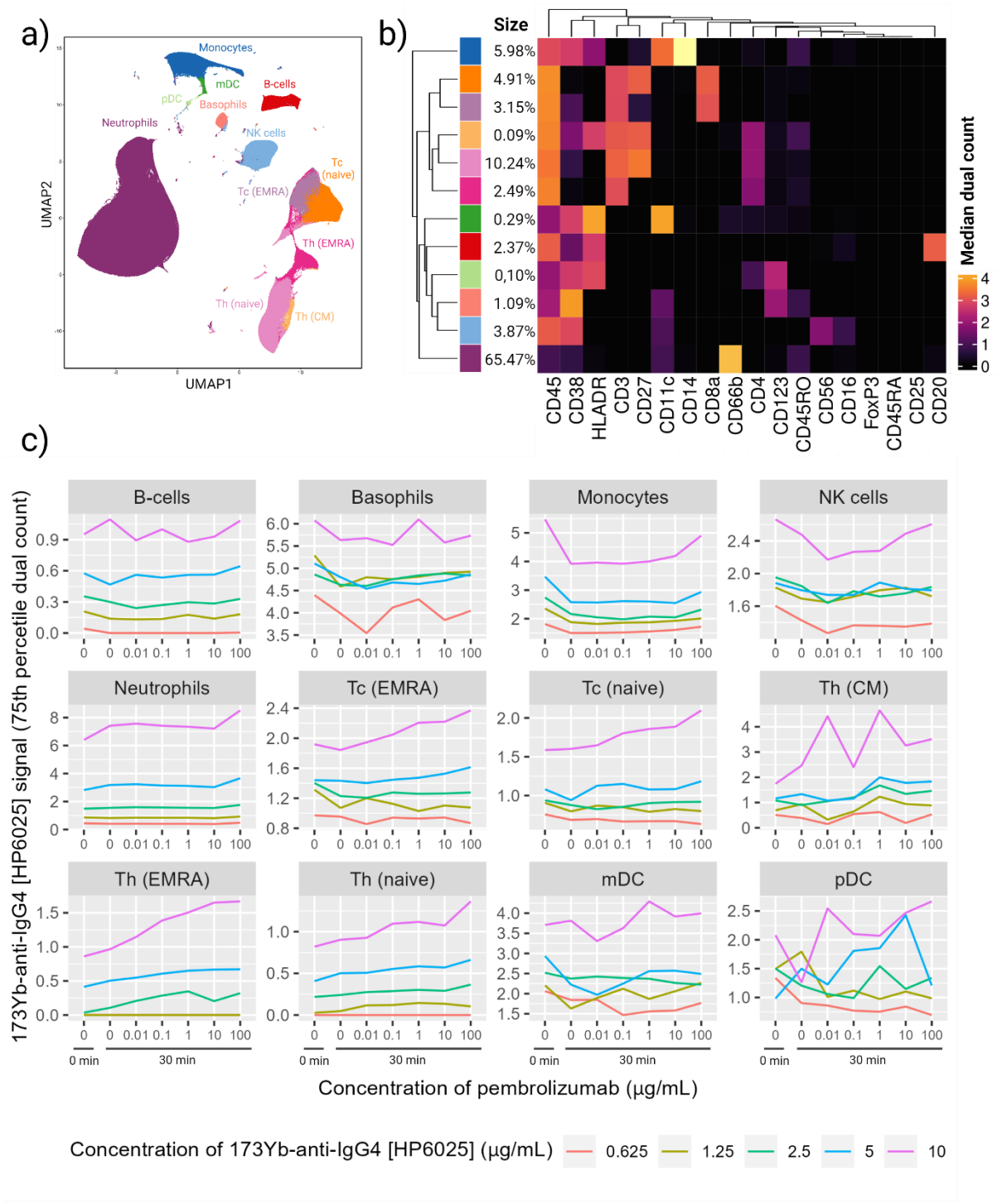

Figure 4.5 Titration plot of 173Yb-anti-IgG4 [HP6025]. a) UMAP showing assigned cell populations from clustering and immunophenotyping. b) Heatmap from showing clusters and markers used for immunophenotyping. c) Signal of 173Yb-anti-IgG4 [HP6025] on the y-axis (be aware of free scales) with increasing incubation concentration (before fixation) of pembrolizumab along the x-axis for donor 1. The different lines correspond to the concentrations of 173Yb-anti-IgG4 [HP6025] used in the titration.

4.2 Receptor Occupancy in Patient Samples

4.2.1 Binding of 166Er-anti-PD-1 [EH12.1] and 173Yb-anti-IgG4 [HP6025] in all Cell Populations

The patient samples were processed and analyzed as described in section 3.6.6. First, the objective was to get an overview of the general binding of 166Er-anti-PD-1[EH12.1] and 173Yb-anti-IgG4[HP6025] in all the different cell populations. For this purpose, a subsample of 10000 cells from each timepoint of each patient was taken and clustered as described in section 3.5.8. The clusters were phenotyped according to UMAP and heatmap showed in Figure 4.6 a) and b), respectively. For each of the cell populations, a mean dual count was calculated for 166Er-anti-PD-1[EH12.1] and 173Yb-anti-IgG4[HP6025] for all patients receiving pembrolizumab and at each timepoint. The results are shown in Figure 4.6 c) together with an UMAP showing the scaled dual count of the two markers (Figure 4.6 d).

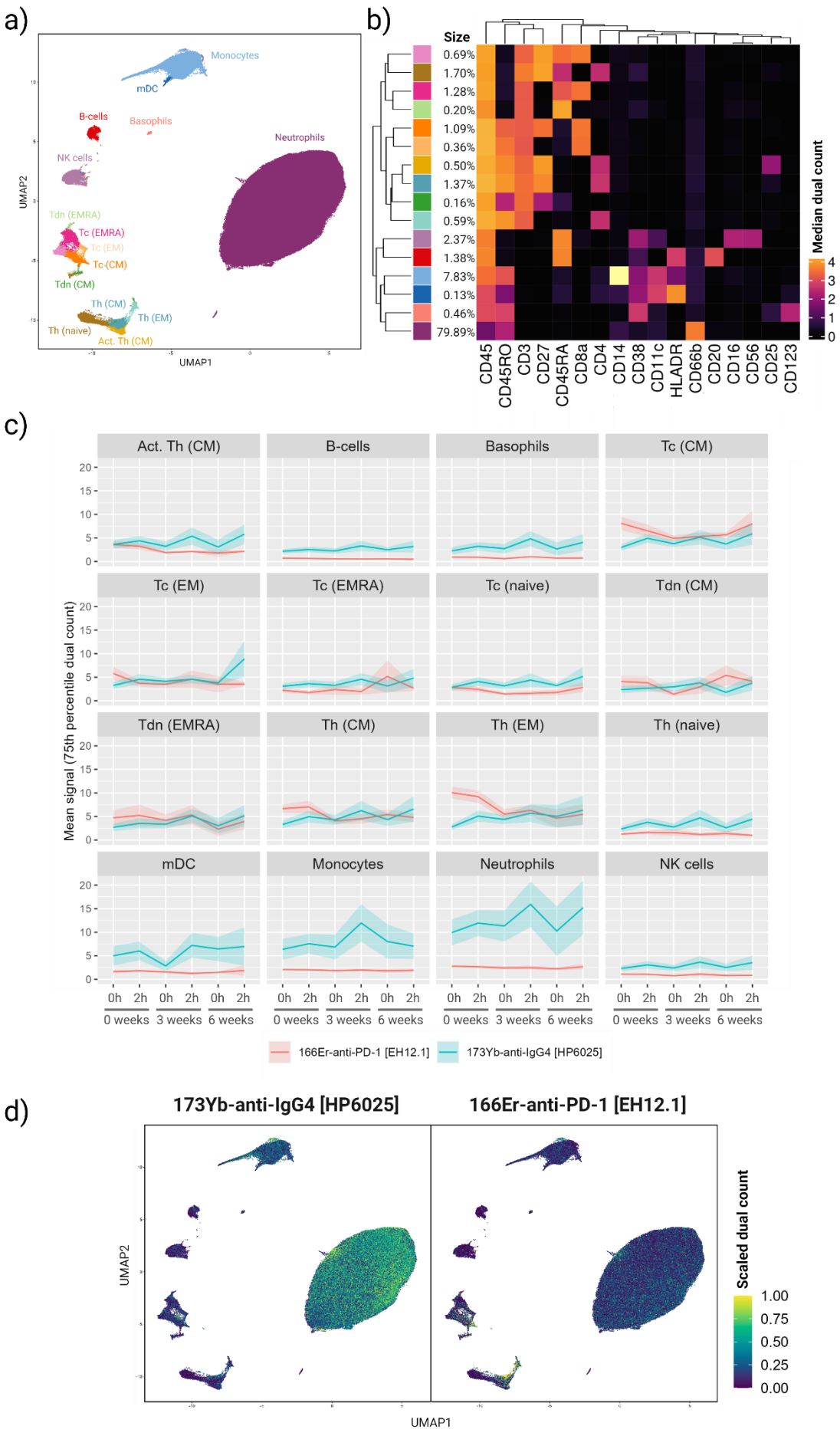
a)
Monocytes
mDC
B-cells
Basophils
Neutrophils
NK cells
Tdn (EMRA)
Tc (EMRA)
Tc (EM)
Tc (CM)
Tdn (CM)
Th (CM)
Th (EM)
Th (naive)
Act. Th (CM)
UMAP2
UMAP1
b)
Size
0.69%
1.70%
1.28%
0.20%
1.09%
0.36%
0.50%
1.37%
0.16%
0.59%
2.37%
1.38%
7.83%
0.13%
0.46%
79.89%
CD45
CD45RO
CD3
CD27
CD45RA
CD8a
CD4
CD14
CD38
CD11c
HLADR
CD66b
CD20
CD16
CD56
CD25
CD123
Median dual count
c)
Act. Th (CM)
B-cells
Basophils
Tc (CM)
Tc (EM)
Tc (EMRA)
Tc (naive)
Tdn (CM)
Tdn (EMRA)
Th (CM)
Th (EM)
Th (naive)
mDC
Monocytes
Neutrophils
NK cells
Mean signal (75th percentile dual count)
0h 2h
0 weeks 3 weeks 6 weeks
166Er-anti-PD-1 [EH12.1]
173Yb-anti-IgG4 [HP6025]
d)
173Yb-anti-IgG4 [HP6025]
166Er-anti-PD-1 [EH12.1]
UMAP2
UMAP1
Scaled dual count
1.00
0.75
0.50
0.25
0.00

Figure 4.6 Results from subsampling 10000 cells from each time point. a) UMAP showing assigned cell populations from clustering and immunophenotyping of all patients. b) Heatmap from clustering showing clusters and markers used for immunophenotyping for all patients. c) Mean dual count of all patients treated with pembrolizumab (y-axis) for 173Yb-anti-IgG4[HP6025] (red line) and 166Er-anti-PD-1 [EH12.1] (blue line) at different timepoints (x-axis). d) UMAP showing scaled dual count of 173Yb-anti-IgG4 [HP6025] and 166Er-anti-PD-1 [EH12.1].

The signal of 166Er-anti-PD-1[EH12.1] seems to be generally lower in the populations that are expected to not express PD-1. Neutrophils show a bit higher signal than the other negative populations, which could be unspecific binding of the antibody, consistent with what was observed in the titration of 166Er-anti-PD-1 [EH12.1] (section 4.1.4). From the UMAP in Figure 4.6 d) it seems that the signal of 166Er-anti-PD-1 [EH12.1] is mainly from the memory T cells, as was the case for 159Tb-pembrolizumab from the results in section 4.1.1. In comparison, 173Yb-anti-IgG4 [HP6025] shows some signal on the memory T cells as well, but also considerable signal on the neutrophils and monocytes. Even in the first sample where there should be no pembrolizumab present, there is a mean signal in all the patients, especially high for neutrophils and monocytes. However, there is a clear zigzag shape of the signal line, showing an increase in signal 2 hours after each new injection of pembrolizumab. This might indicate that 173Yb-anti-IgG4 [HP6025] still could still be useful in detecting relative changes in bound pembrolizumab with time, so further assessment of this antibody in the patient samples was conducted.

Figure 4.7 a) shows the signal of 173Yb-anti-IgG4 [HP6025] for the first timepoint (before any injection with pembrolizumab) for the healthy donor and all patients, including the patient who received atezolizumab and the patient who received lytix. Almost all patients and the healthy donor show binding of 173Yb-anti-IgG4 [HP6025] in all cell populations even though there is no IgG4-drug injected at this timepoint in any of the samples. The signal in neutrophils and monocytes seems to be quite high for all patients and the healthy donor. Longitudinal data spanning over several treatment cycles was available for patient 10, who received atezolizumab. Since atezolizumab is not an IgG4-based drug, these data could reveal how the signal of 173Yb-anti-IgG4 [HP6025] changes with time. This is shown in Figure 4.7 b). Here, we see that the signal is approximately the same for the different sample timepoints in each population. Based on this, it was decided that 173Yb-anti-IgG4 [HP6025] was to be included in the analysis of receptor occupancy as a reporter for the relative change in the signal of bound pembrolizumab. Since the signal of 173Yb-anti-IgG4 [HP6025] in the atezolizumab patient in Figure 4.7 b) seemed to be quite stable over time, the signal in the first sample of all pembrolizumab patients was assumed to be representative of the expected signal in the consecutive samples for that patient. Therefore, this first signal was subtracted from the other samples belonging to the same patient.

a)

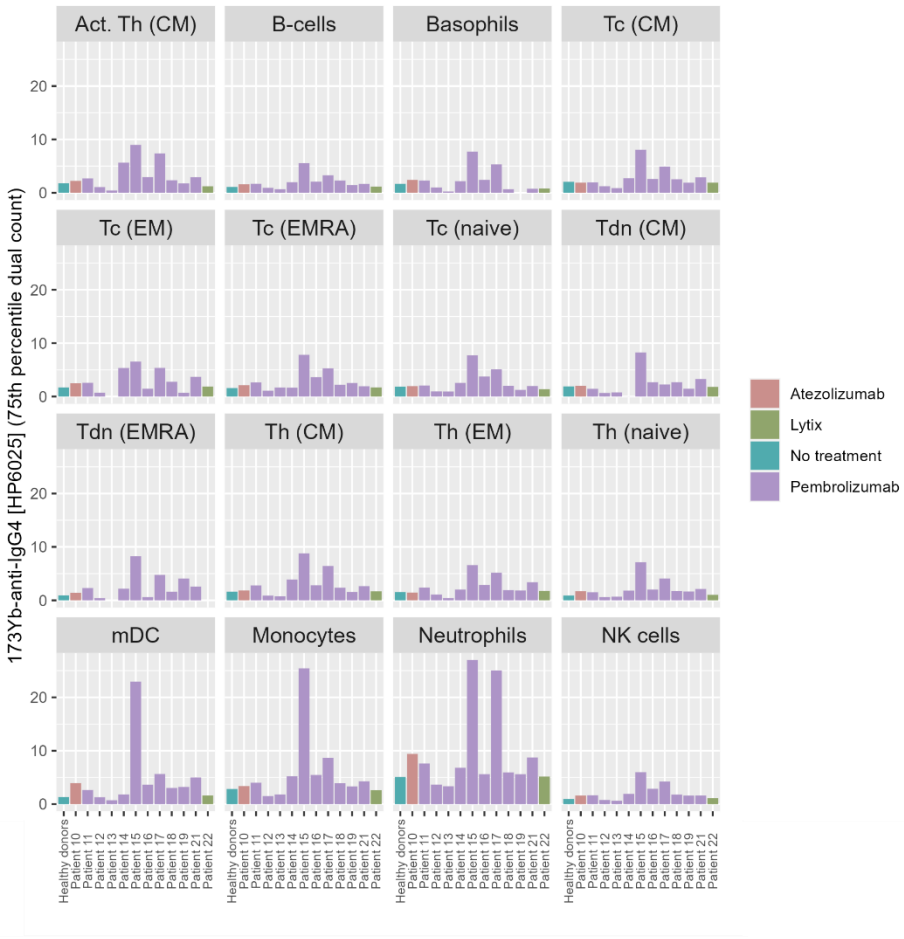
Act. Th (CM)
B-cells
Basophils
Tc (CM)
Tc (EM)
Tc (EMRA)
Tc (naive)
Tdn (CM)
Tdn (EMRA)
Th (CM)
Th (EM)
Th (naive)
mDC
Monocytes
Neutrophils
NK cells
173Yb-anti-IgG4 [HP6025] (75th percentile dual count)
Atezolizumab
Lytix
No treatment
Pembrolizumab
Healthy donors
Patient 10
Patient 11
Patient 12
Patient 13
Patient 14
Patient 15
Patient 16
Patient 17
Patient 18
Patient 19
Patient 21
Patient 22

b)

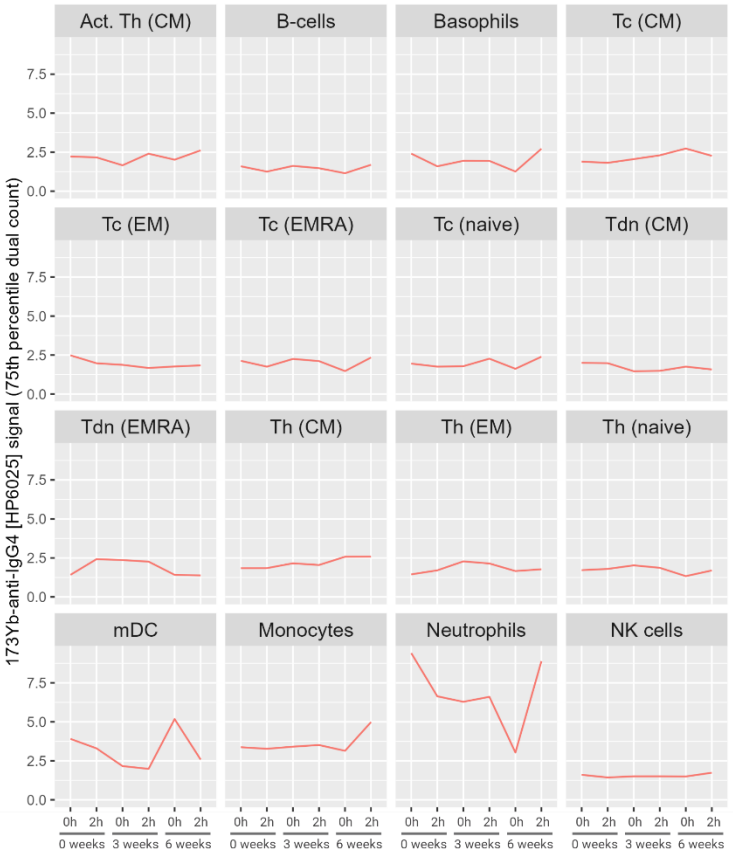
Act. Th (CM)
B-cells
Basophils
Tc (CM)
Tc (EM)
Tc (EMRA)
Tc (naive)
Tdn (CM)
Tdn (EMRA)
Th (CM)
Th (EM)
Th (naive)
mDC
Monocytes
Neutrophils
NK cells
173Yb-anti-IgG4 [HP6025] signal (75th percentile dual count)
0h
2h
0 weeks
3 weeks
6 weeks

Figure 4.7 Investigation of 173Yb-anti-IgG4 [HP6025] signal. a) Barplot showing signal of 173Yb-anti-IgG4 [HP6025] at first timepoint (0 weeks, 0 h) before injection with drug for all patients and healthy donor control. b) Signal of 173Yb-anti-IgG4 [HP6025] and in patient receiving treatment with atezolizumab, a non-IgG4 drug.

4.3.2 Receptor Occupancy in Patient Samples

For the calculation of receptor occupancy in the patients having received treatment with pembrolizumab, T cells were first manually gated. Then, the gated subsample of T cells was clustered using the FlowSOM algorithm and a dimensionality reduction was conducted. The result of the clustering and dimensionality reduction is shown in the UMAP and heatmap in Figure 4.8 a) and b). The scaled dual count of the two antibodies is also shown in a UMAP in Figure 4.8 a). The receptor occupancy was calculated for all patients in each cell population. Figure 4.8 c) shows the mean dual count and mean of the calculated receptor occupancy of all the patients for a selection of the T cells (only central memory cells). All memory T cell subsets showed similar patterns as the ones seen in Figure 4.8 c), therefore, only a selection of the cells is shown in the results. Since only a small selection of the patients had samples collected after treatment cycle 3 (9 weeks), Figure 4.8 c) only shows the mean expression and receptor occupancy of the first 3 cycles.

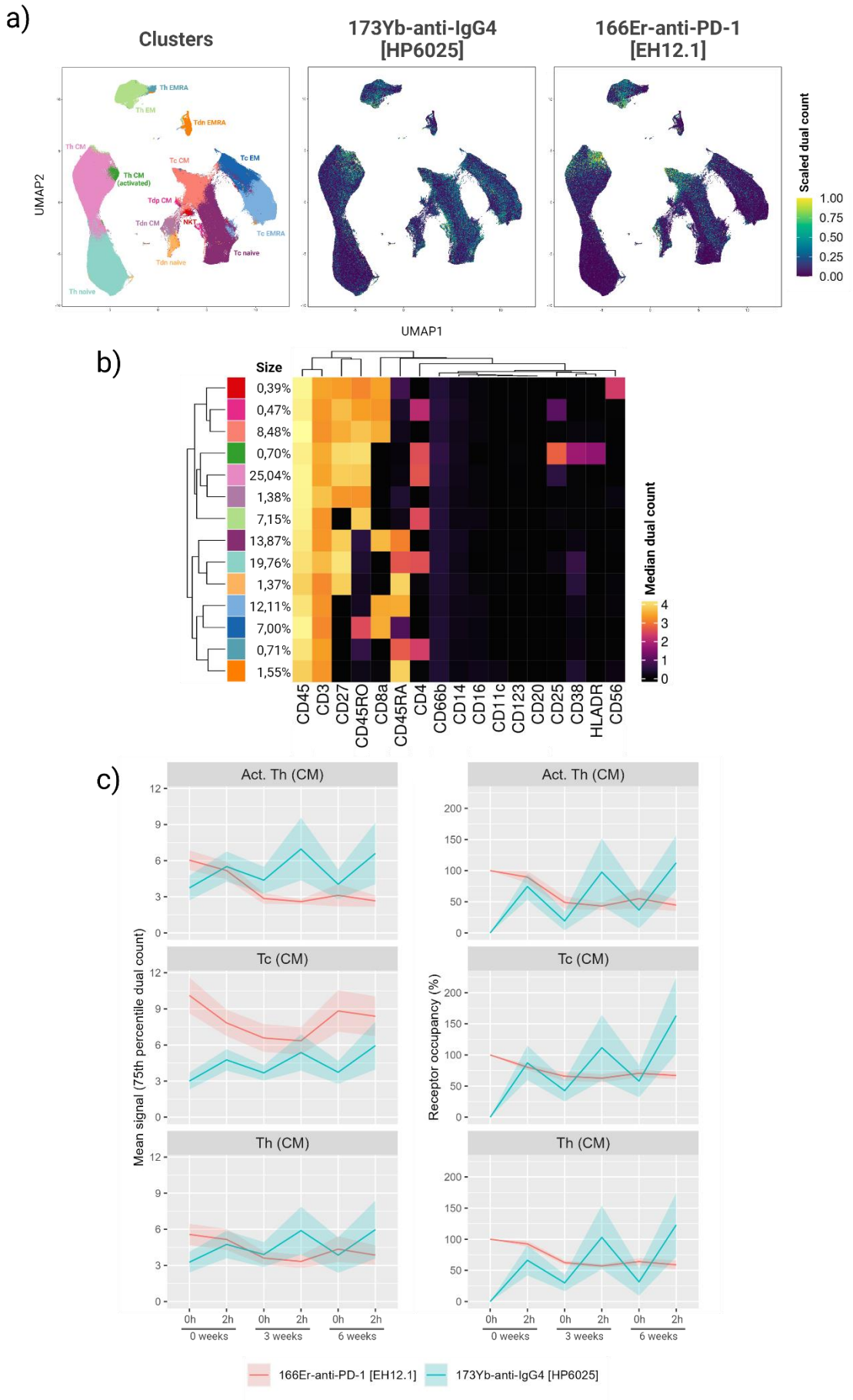
a)
Clusters
173Yb-anti-IgG4 [HP6025]
166Er-anti-PD-1 [EH12.1]
Th EMRA
Th EM
Tdn EMRA
Th CM
Tc CM
Tc EM
Th CM (activated)
Tdp CM
Tdn CM
NKT
Tc EMRA
Tc naive
Tdn naive
Th naive
UMAP2
UMAP1
Scaled dual count
1.00
0.75
0.50
0.25
0.00
b)
Size
0,39%
0,47%
8,48%
0,70%
25,04%
1,38%
7,15%
13,87%
19,76%
1,37%
12,11%
7,00%
0,71%
1,55%
CD45
CD3
CD27
CD45RO
CD8a
CD45RA
CD4
CD66b
CD14
CD16
CD11c
CD123
CD20
CD25
CD38
HLADR
CD56
Median dual count
4
3
2
1
0
c)
Act. Th (CM)
Tc (CM)
Th (CM)
Mean signal (75th percentile dual count)
Receptor occupancy (%)
0h
2h
0 weeks
3 weeks
6 weeks
166Er-anti-PD-1 [EH12.1]
173Yb-anti-IgG4 [HP6025]

Figure 4.8 Immunophenotyping and calculated receptor occupancy of CD3-gated patient samples. a) Shows UMAP of the assigned populations to the clusters and two UMAPs showing scaled dual count of 173Yb-anti-IgG4 [HP6025] or 166Er-anti-PD-1 [EH12.1]. b) Heatmap showing median expression of markers used in immunophenotyping of the clusters. c) Mean dual count and mean receptor occupancy for all patients having received pembrolizumab. The plot only shows the central memory T cell populations and 6 samples, corresponding to 3 treatment cycles, but similar patterns are seen in the other memory T cell populations.

From Figure 4.8 c), one can clearly see a decrease in signal of 166Er-anti-PD-1 [EH12.1] corresponding in a decrease in available receptors, suggesting an increased receptor occupancy of pembrolizumab. Thus, the trend for the mean of all the patients is that less PD-1 receptors are available after injection with pembrolizumab, and this difference can be measured already 2 hours after injection. Correspondingly, the mean dual count of 173Yb-anti-IgG4 [HP6025] is increasing with time. The signal is reduced from the 2 hours-sample to the 0-hours sample in the next treatment cycle, creating the zigzag-shape of the blue line. Nevertheless, the overall signal is increasing with time, but the relative change in signal is considerable already 2 hours after injection as well. Thus, both approaches seem to be able to measure an increase in receptor occupancy on PD-1 by pembrolizumab on memory T cells, just 2 hours after injection.

Figure 4.9 shows the calculated receptor occupancy for every patient (grey lines) and the mean receptor occupancy (red line) for the three central memory T cell populations. The figure displays results from each of the antibodies separately in Figure 4.9 a) and b). Looking at the signal of 166Er-anti-PD-1 [EH12.1] in the first sample (0 h, 0 weeks) reveals that there is a large range in the baseline dual count of each patient. Thus, using this first sample as a reference visualizes the relative decrease in available receptors. However, there are still some patients who deviate from this pattern, and even have a slight increase in the detected receptors between the 0 hours and 2 hours-sample in the first treatment cycle. Since there are no available samples of these patients after the treatment cycle, it is hard to say if this lack of decrease in signal is a trend for the patient or is just limited to the first sample after injection.

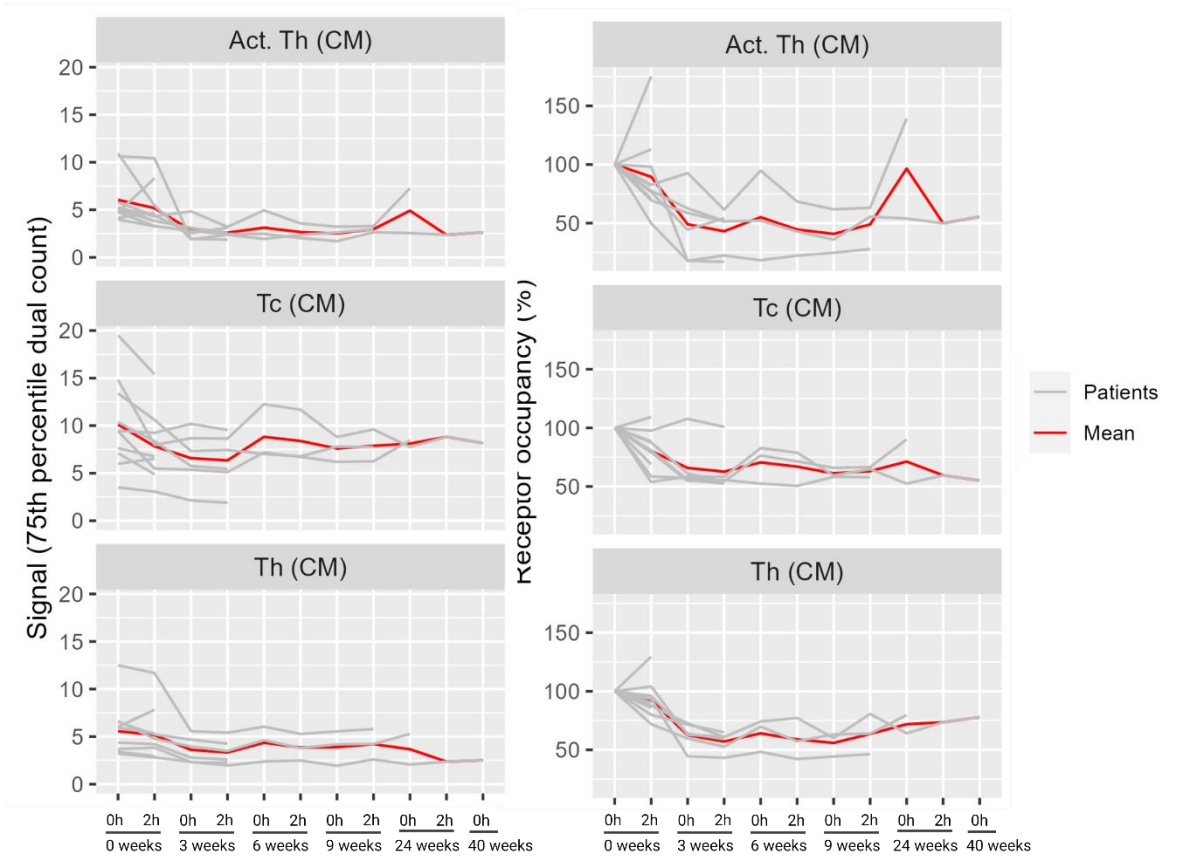
Act. Th (CM)
Tc (CM)
Th (CM)
Signal (75th percentile dual count)
Receptor occupancy (%)
Patients
Mean
0h 2h
0 weeks
3 weeks
6 weeks
9 weeks
24 weeks
40 weeks

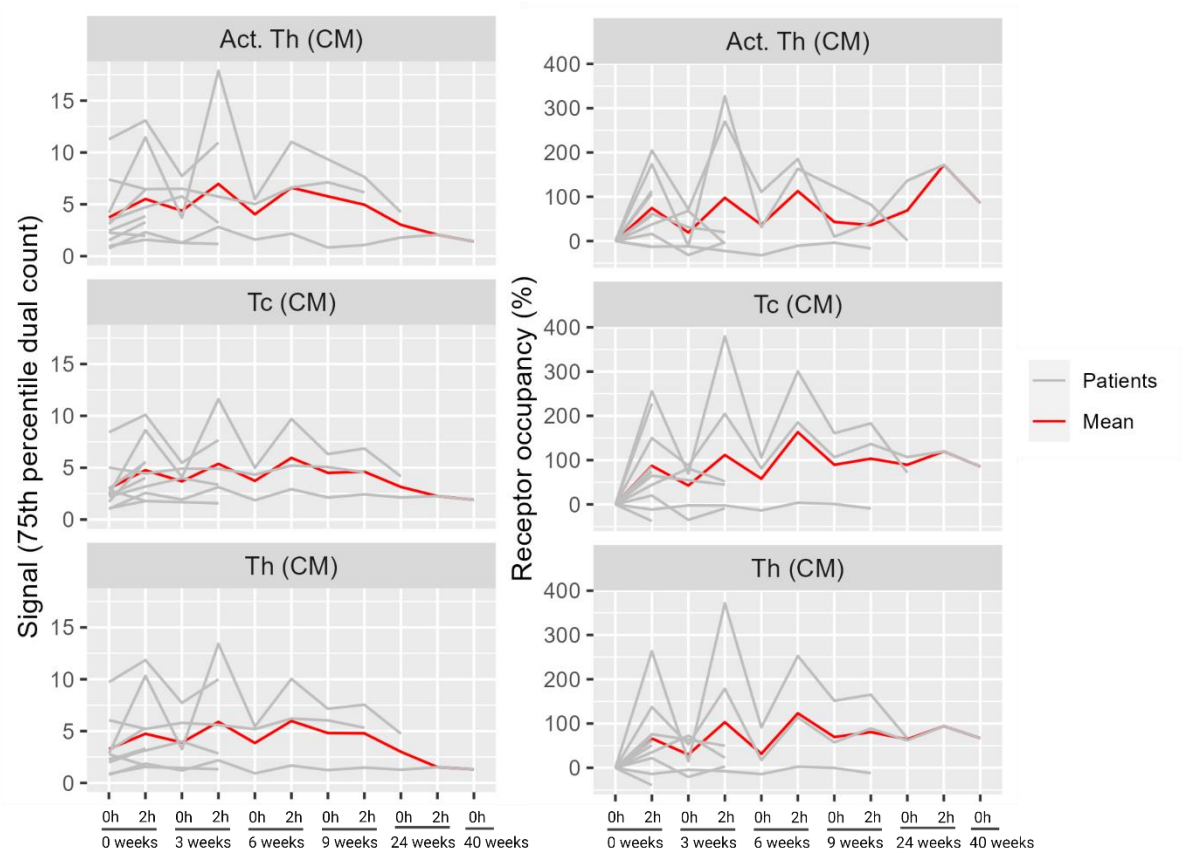
Act. Th (CM)
Tc (CM)
Th (CM)
Signal (75th percentile dual count)
Receptor occupancy (%)
Patients
Mean
0h 2h
0 weeks
3 weeks
6 weeks
9 weeks
24 weeks
40 weeks

Figure 4.9 Signal and receptor occupancy for each patient and the calculated mean. a) Shows dual count and receptor occupancy for 166Er-anti-PD-1 [EH12.1] in the central memory T cells for all patients and the calculated mean of all these. b) Shows dual count and receptor occupancy for 173Yb-anti-IgG4 [HP6025] in the central memory T cells for all patients and the calculated mean of all these.

The signal of 173Yb-anti- IgG4 [HP6025] is also quite variable for each of the patients in the first sample. It is also clear from this plot showing signal or increasing relative change in receptor occupancy of each patient that not all lines follow the zigzag shape. Some patients are just missing samples spanning further than the first cycle, but some just have minor or no change in the signal of 173Yb-anti- IgG4 [HP6025] throughout the treatment cycles. Three patients (Patient 13, 14 and 17) that had the most longitudinal data available were chosen to further visualize this effect. Their dual count and receptor occupancy for both antibodies are shown in Figure 4.10. Patients 13 and 14 have quite different dual count for 173Yb-anti-IgG4 [HP6025], but their relative change in receptor occupancy are quite similar. Patient 17 stands out with virtually no change in 173Yb-anti-IgG4 [HP6025] throughout the treatment. Interestingly, patient 17 has a significant drop in signal of 166Er-anti-PD-1 [EH12.1] after the first treatment cycle, especially in the helper T cells. Even though there is a decrease for the two other patients as well, it is not as large as for patient 17.

a)

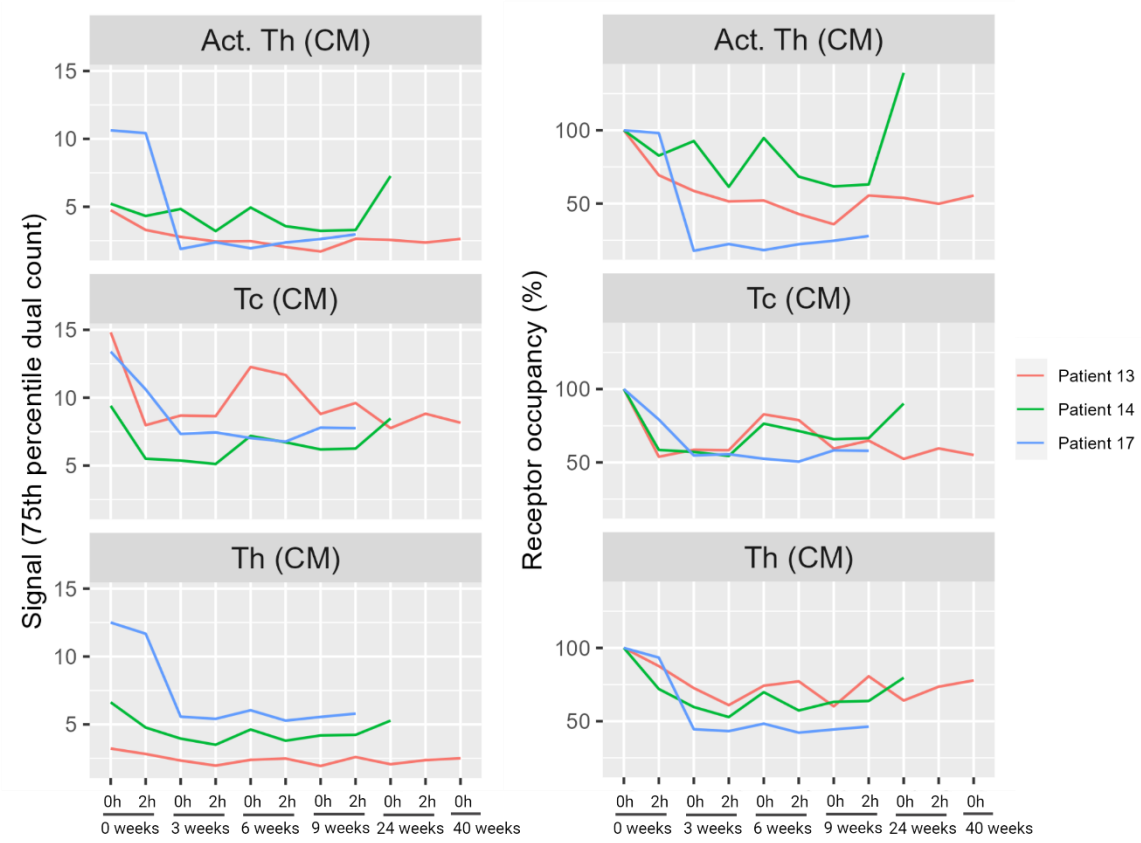
166Er-anti-PD-1 [EH12.1]
Act. Th (CM)
Tc (CM)
Th (CM)
Signal (75th percentile dual count)
Receptor occupancy (%)
Patient 13
Patient 14
Patient 17
0h 2h
0 weeks
3 weeks
6 weeks
9 weeks
24 weeks
40 weeks

b)

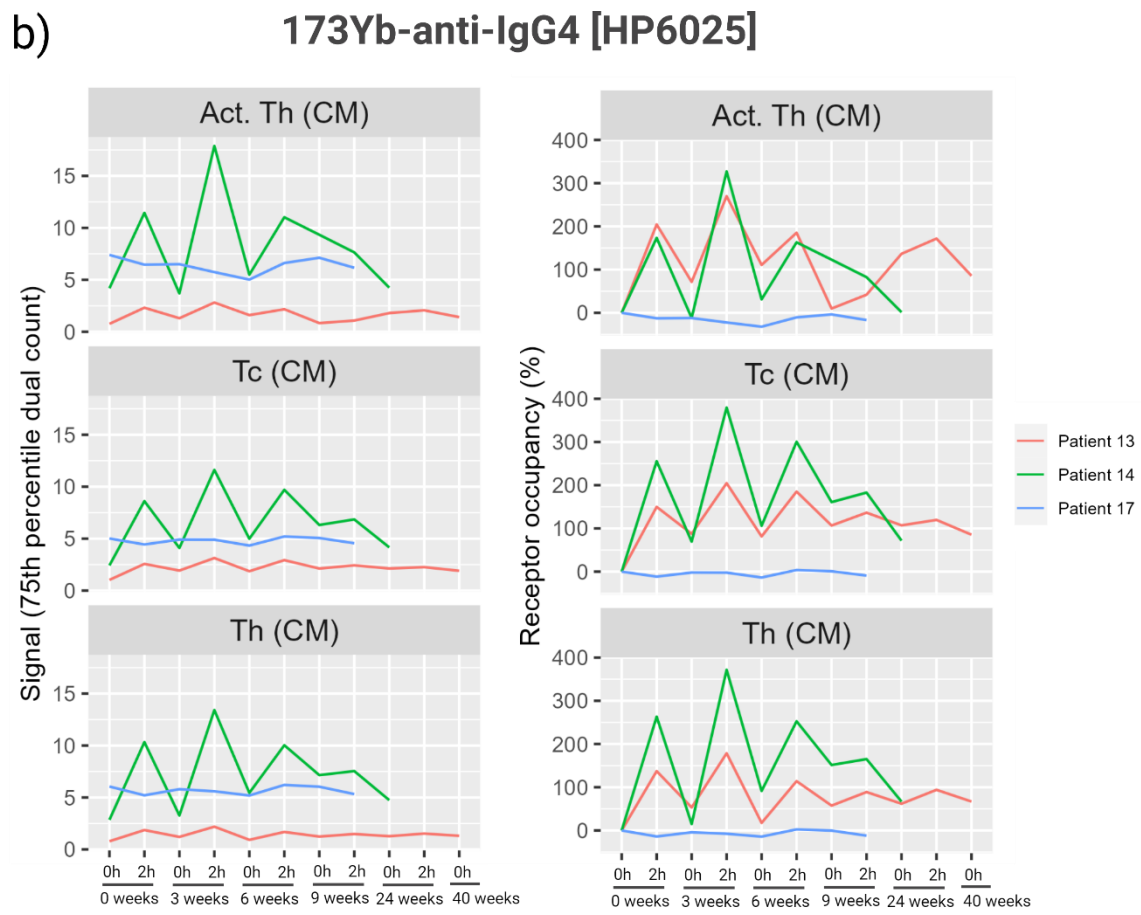
173Yb-anti-IgG4 [HP6025]
Act. Th (CM)
Tc (CM)
Th (CM)
Signal (75th percentile dual count)
Receptor occupancy (%)
Patient 13
Patient 14
Patient 17
0h 2h
0 weeks
3 weeks
6 weeks
9 weeks
24 weeks
40 weeks

Figure 4.10 Signal and receptor occupancy patients 13, 14 and 17. a) Shows signal and receptor occupancy for 166Er-anti-PD-1 [EH12.1] in the central memory T cells for patients 13, 14 and 17. b) Shows signal and receptor occupancy for 173Yb-anti-IgG4 [HP6025] in the central memory T cells for patients 13, 14 and 17.

4.3.3 Preliminary Statistical Analysis

The measured dual counts and calculated receptor occupancies was used to conduct a t-test to check if there was any significant difference between the means of the dual counts or receptor occupancy of responders and non-responders as described in section 3.8. The results are shown in Table. 4.1. The distributions and mean of responders and non-responders are shown for one of the cell populations (helper T cells (CM)) in Figure 4.11. No p-value for any of the antibodies, cell populations or types of values measured are lower than 0,05. That means that the null hypothesis was not rejected. There seems to be no significant difference in any of the means for the responders and non-responders.

Table 4.1 P-values calculated from t-test of responders vs non-responders. t-tests were conducted for both antibodies, for three cell populations and for the dual count and calculated receptor occupancy of each of these. The p-values from the F-test were used to decide if an equal variance t-test or an unequal variance t-test was to be used on the two sets of values. The p-value from the t-test was used to decide if there was any significant difference in the mean between the responders and non-responders.

Antibody	Cell population	Type of value	p-value (F-test)	p-value (t-test)
166Er-anti-PD-1 [EH12.1]	Activated helper T cells (CM)	Dual count	0,0202	0,2671
		Receptor occupancy	0,2146	0,2460
	Cytotoxic T cells (CM)	Dual count	0,3783	0,1150
		Receptor occupancy	0,6702	0,4373
	Helper T cells (CM)	Dual count	0,0545	0,0683
		Receptor occupancy	0,4209	0,1465
173Yb-anti-IgG4 [HP6025]	Activated helper T cells (CM)	Dual count	0,2293	0,1973
		Receptor occupancy	0,6241	0,2734
	Cytotoxic T cells (CM)	Dual count	0,3719	0,2736
		Receptor occupancy	0,6600	0,5227
	Helper T cells (CM)	Dual count	0,1331	0,2363
		Receptor occupancy	0,3627	0,1983

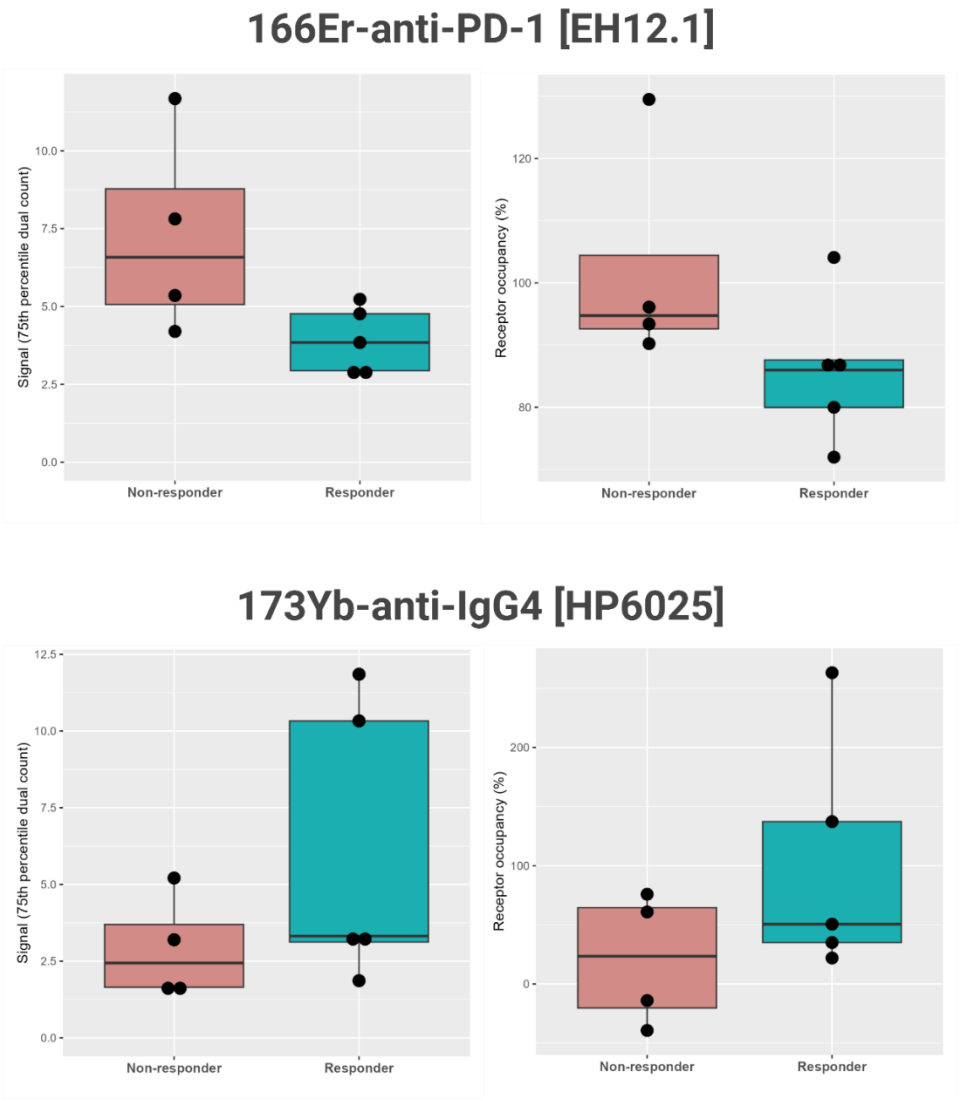

Figure 4.11 Boxplot of the distribution and mean of responders and non-responders for helper T cells (CM).

4.4 Test of QSC Beads on CyTOF XT®

Quantum™ Simply Cellular® (QSC) beads were tested for the antibody 166Er-anti-PD-1 [EH12.1] as described in section 3.7. If the mass cytometer was able to detect all beads, it would be possible to create a standard curve from the dual count and the corresponding known Antibodies Bound per Cell (ABC) for each of the bead populations. Then each detected dual count of 166Er-anti-PD-1 [EH12.1] could be transformed to a total number of antibodies bound to each cell and would help standardize the measurement of receptor occupancy. The results from the test are shown in Figure 4.12. Beads 3 and 4 seem to be well separated and have different dual counts as they should have. However, beads 1 and 2 cannot be distinguished from bead 3 or each other. They seem to be on the limit of the event length detected by the mass cytometer.

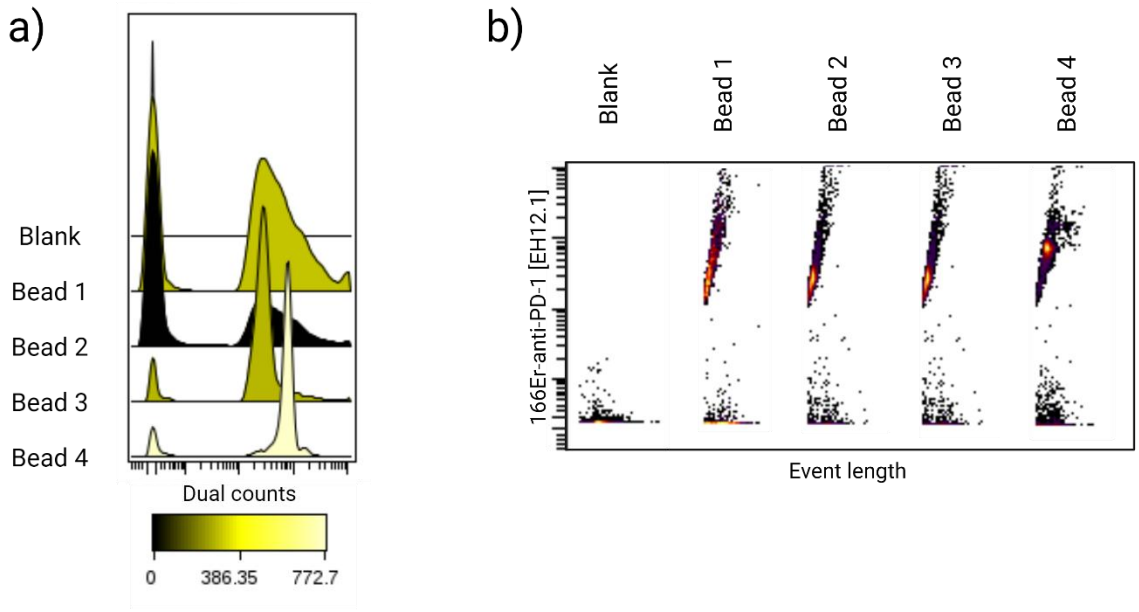

Figure 4.12 Results from test of QSC beads. a) Histogram showing dual counts of 166Er-anti-PD-1 [EH12.1] for the blank and four QSC bead populations. b) Dot plot showing dual count of 166Er-anti-PD-1 [EH12.1] in each of the QSC bead populations.

4.4 Induced Expression of PD-1 on Jurkat cells

Jurkat cells were intended to be used as positive and negative biological control in the assay. Jurkat cells do not normally express PD-1, so to induce this expression, a method described by Yang et al. (2008) was tested [74]. Herein, the cells were stimulated with 1 µg/mL PHA and 50 ng/mL PMA for 48 hours. Following fixation, the cells were stained with four metal conjugated antibodies: 111Cd-anti-CD3 [UCHT1], 145Nd-anti-CD4 [RPA-T4], 157Gd-anti-CD8a [HIT8A], and 166Er-anti-PD-1 [EH12.1]. The results revealed considerable expression of CD3 and CD4 but not CD8 in both stimulated and unstimulated cells. Expression of PD-1 was successfully induced but only for 1,31% of the cells (Figure 4.1).

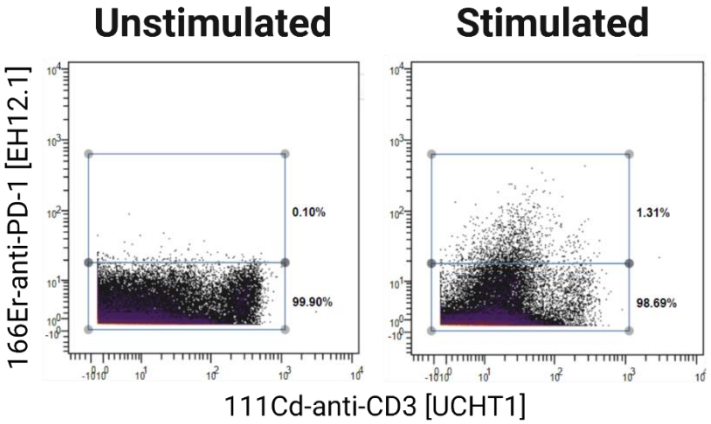

Figure 4.1 Biaxial plot showing signal of 166Er-anti-PD-1 [EH12.1] and 11Cd-anti-CD3 [UCHT1] on stimulated and unstimulated Jurkat cells. PD-1 was successfully induced, but only for 1,31% of the cells.

5 Discussion

This thesis aimed to develop a mass cytometry panel that could measure the receptor occupancy of PD-1 by pembrolizumab. A panel was successfully developed, using 173Yb-anti-IgG4 [HP6025] and 166Er-anti-PD-1 [EH12.1] for a bound receptors and free receptors approach, respectively. The panel was tested on samples from patients having received treatment with pembrolizumab. Both approaches were able to measure an increase in the receptor occupancy of PD-1 after starting treatment with pembrolizumab in most of the patients. For many patients, the change in receptor occupancy was detectable already 2 hours after injection. Preliminary statistical analysis indicates that there is no significant difference in the receptor occupancy in responders and non-responders for the group of patients studied in this thesis.

5.1 Development of Receptor Occupancy Panel

5.1.1 Considerations for Pembrolizumab

Pembrolizumab is a therapeutic antibody that targets PD-1. The results from section 4.1.1 show specific binding of 159Tb-pembrolizumab to T cells, as expected since PD-1 is mainly expressed on activated T- and B-cells [25]. No expression in the B-cells was observed. Since the in-house panel was intended to investigate T cell compartments, the B-cells were not gated based on their activation. Thus, the signal shown is for all B-cells, and could explain why there is no observed binding of 159Tb-pembrolizumab. The saturation of 159Tb-pembrolizumab was found to be 1 µg/mL, also relatively consistent with previous findings of pembrolizumab being saturated at 0,5 µg/mL [65].

The competition assay also revealed an increased signal from the PD-1 antibody [EH12.1] in samples incubated with unconjugated pembrolizumab than in samples incubated with 159Tb-pembrolizumab. A possible cause for this can be that less 159Tb-pembrolizumab is bound to the cells than unconjugated pembrolizumab. This could be due to loss in affinity or steric hindrance when there is a polymer loaded with metals attached to the antibody. Another possible cause could be that 166Er-anti-PD-1 [EH12.1] is outcompeting the conjugated pembrolizumab for the PD-1 receptor. In this case, even if the same amount of conjugated and unconjugated pembrolizumab was bound, the conjugated pembrolizumab would experience more dissociation and competition from 166Er-anti-PD-1 [EH12.1]. These results were crucial in deciding which PD-1 antibody clone to use in the free receptors approach, as elaborated in section 4.1.3.

5.1.2 Considerations for Antibodies

The results from the competition assay in section 4.1.3 revealed that the 168Er-anti-PD-1 [MIH4] seemed not to work well in detecting PD-1 as it seems to bind to cell populations that are not expected to express PD-1. In addition, it does not reach a saturation as the two other clones do and it is not affected by pembrolizumab being bound to the cell. Zelba et al. (2019) found that both EH12.2H7 and MIH4 compete against pembrolizumab in binding to PD-1, but that MIH4 still can detect some PD-1 receptors even in the presence of pembrolizumab [80]. This could be in agreement with what was found in the competition assay in this thesis. The samples in the study mentioned above were fixed after extracellular antibody staining. Thus, another possible cause for unspecific binding is that the epitopes of PD-1 is changed during the

fixation, and thus reducing the binding of the MIH4 clone. Conducting an experiment comparing the receptor occupancy derived from staining live cells and staining after fixation would be necessary to determine the effect of the fixation.

One approach in calculating receptor occupancy was to use an antibody against IgG4 to detect PD-1 bound pembrolizumab, as pembrolizumab itself is an IgG4 antibody. Both in the samples from healthy donors and patients, we were able to detect considerable IgG4 signal in several cell populations without any prior treatment with pembrolizumab. Especially neutrophils and monocytes had high signals of the secondary antibody. There are several possible explanations for this observed binding to other cell populations. The antibody could bind unspecifically or not work on fixed cells. Another possible explanation could be that pembrolizumab is binding to other cell types, and that 173Yb-anti-IgG4 [HP6025] is detecting this pembrolizumab. The results in section 4.1.1 showed that conjugated pembrolizumab binds specifically to T cells and did not have significant signal in the other cell populations. Still, from Figure 4.2 d) one can see that the expression of 159Tb-pembrolizumab is increasing in neutrophils at a concentration of 10 µg/mL, which could indicate that unspecific binding starts for pembrolizumab at approximately this concentration. The median trough concentrations in plasma when pembrolizumab is in steady-state is around 22-29 µg/mL [3]. Therefore, it is possible that the concentration of pembrolizumab found in the peripheral blood of patients is high enough for some of the pembrolizumab to bind to other cell types as well.

Since 173Yb-anti-IgG4 [HP6025] is a secondary antibody that is not specific only for pembrolizumab, but all IgG4 antibodies, yet another explanation could be that the antibody is detecting other IgG4 antibodies bound to the cells. As it turns out, cell surface receptors called Fc gamma receptors (FcγR) can bind to the Fc domain of IgG antibodies. These receptors are divided into several subgroups: FcγRI (CD64), FcγRII (CD32), FcγRIII (CD16) and FcγRIV (CD16-2). Amongst some of the cell types where we were able to detect considerable IgG4 signal are neutrophils, monocytes, natural killer cells and myeloid dendritic cells. According to Nimmerjahn and Ravetch (2008), neutrophils mainly express FcγRIIB, FcγRIII and FcγRIV, dendritic cells express FcγRI, FcγRIIB, and FcγRIII while monocytes express all the subgroups. Natural killer cells only express FcγRIII and B-cells only FcγRIIB. The authors state that despite initial studies that indicated that some T cell subsets expressed FcγRs, more recent findings indicate that this is not the case, but they conclude with this statement: "The question of T cell expression of FcγRs is, however, best considered to be an open one, as it is notoriously difficult to examine every possible subset or activation state of T cells for FcγR expression"[15]. However, BioLegend lists macrophages, monocytes, neutrophils, NK-cells and T cells as the cell types under the antigen details of the anti-human CD16 (FcγRIII) antibody used in the panel of this thesis [81]. This indicates that T cells also can express at least one of the FcγRs.

From the results shown in Figure 4.7 we can see that the IgG4 signal is highest in the neutrophils, closely followed by monocytes and myeloid dendritic cells. Natural killer cells also have significant signal, while B-cells have a bit lower signal. Since B-cells have lower IgG4 signal and is mainly expressing FcγRIIB of the FcγRs, the common denominator for all the other populations is FcγRIII (CD16). If we look at the heatmap in Figure 4.5 b) from the titration

of 173Yb-anti-IgG4 [HP6025] on healthy donors, we can see that both NK-cells express CD16 as expected. From Figure 4.6 b) for the patient samples, also NK cells that shows expression of CD16. The CD16 clone used in this thesis does not detect CD16 on neutrophils when the cells are fixed. Therefore, we do not except to see any signal on neutrophils in Figure 4.5 b) and 4.6 b). This could support the explanation that 173Yb-anti-IgG4 [HP6025] is measuring IgG4 bound to FcγRs on different cell populations in addition to pembrolizumab. In figure 4.6 c), all cell populations seem to follow the same pattern with a zigzag shape of the signal intensity of IgG4. There is evidence supporting both explanations, so further analysis is necessary conclude exactly what is causing the binding of 173Yb- anti-PD-1 [HP6025] on the other cell populations. It could also be that the correct explanation is, in fact, a combination of both effects.

As shown in the samples from patient 11 receiving treatment with pembrolizumab in Figure 4.7 b), it seems that the signal of 173Yb-anti-IgG4 [HP6025] remains stable with time, even for weeks between each treatment cycle. Based on this, the baseline signal of 173Yb-anti-IgG4 [HP6025] in the sample before treatment with pembrolizumab was assumed to be the same in the other samples. The signal of the first sample was subtracted from the signal in the other samples, and the remaining increase in signal was considered to be caused by pembrolizumab binding to the cells. This assumption might affect the accuracy of the measurements, as one cannot know with certainty that the signal remains the same with time. In addition, dividing by the signal of the first sample to get a receptor occupancy only provides a relative change in occupancy rather than an absolute change. Ideally, the samples should be divided by a sample that is known to detect 100 % of the PD-1 receptors.

5.2 Receptor Occupancy in Mass Cytometry

5.2.1 Mass Cytometry for Receptor Occupancy Measurements

As stated by Kanutte Huse (2019), the use of mass cytometry can provide new possibilities in measuring the receptor occupancy of complex biological systems [62]. The limited spectral overlap in mass cytometry could provide more accurate receptor occupancy measurements and additionally allows for higher multiplexing of antibodies compared to flow cytometry. This could enable more cell subsets to be identified or allow for increased investigation of functional effects. Bringeland et al. (2020) developed a mass cytometry receptor occupancy assay for natalizumab, a monoclonal antibody used in treating patients with relapse-remitting multiple sclerosis [80]. They were able find an association between low receptor occupancy of natalizumab and a wearing-off effect at the end of the dosing, challenging previous findings conducted with flow cytometry that found no such association [81]. The study using flow cytometry measured receptor occupancy in two cell subsets. In comparison, Bringland et al. (2020) was able to measure the receptor occupancy in 11 cell subsets simultaneously by utilizing mass cytometry. This demonstrates that mass cytometry can be a useful tool in determining receptor occupancy, offering measurement of more complex cell types and possibly revealing biological effects that would otherwise have been missed by flow cytometry.

In line with this, we wanted to use mass cytometry in estimating the receptor occupancy by pembrolizumab. From Figure 4.8 and 4.9 we can see that the developed assay in this thesis

succeeded in estimating receptor occupancies of PD-1 by pembrolizumab in patient samples. To my knowledge this is the first receptor occupancy assay targeting PD-1 for the mass cytometry platform. The receptor occupancies measured in this thesis seem to be lower than those measured in other flow cytometry assays. In a patient achieving full remission after one treatment with pembrolizumab, Osa et al. (2019) detected PD-1 before treatment, but eight weeks after the signal of PD-1 was reduced and instead IgG4 was detected. For most of the patients in this thesis, the receptor occupancy measured by 166Er-anti-IgG4 [EH12.1] was not higher than 50 % nine weeks after the first dose. Additionally, Pluim et al. (2019) measured the receptor occupancy of pembrolizumab to be approximately 95% and 92% on helper T cells and cytotoxic T cells, respectively [65]. This could indicate that the receptor occupancies measured in this thesis is an underestimation of the actual receptor occupancies. Causes for this could be that the EH12.1 clone has higher affinity than pembrolizumab or that the fixation interferes with the binding efficiency of pembrolizumab. An option would be to use 159Tb-pembrolizumab to detect the free receptors as this is the conjugate of the drug. This would possibly give a more accurate estimate of the maximum binding capacity of pembrolizumab. 173Yb-anti-IgG4 [HP6025] is currently estimating a relative change in the receptor occupancy and not an absolute change. Thus, it is difficult to compare the values derived from this antibody to the ones found in literature.

Even though there are several advantages with using mass cytometry for receptor occupancy measurements, the technology also has its limitations compared to flow cytometry. The throughput of mass cytometry, limited to around 400 cells per second, is still 25-50-fold lower than the throughput in flow cytometry [53]. Mass cytometry generally have higher costs than flow cytometry [84]. The sample transmission efficiency is generally lower as well [53]. Still, the possibility of high multiplexing and investigation of more cell subsets could be vital when assessing if receptor occupancy can be used to predict response. The relation of receptor occupancy to response could be in a subset of cells that otherwise could have been missed by analysis with flow cytometry. Consequently, mass cytometry is definitely a useful alternative when determining which analysis technology to use for measuring receptor occupancy.

5.2.2 QSC Beads in Mass Cytometry Receptor Occupancy Measurement

Despite the high accuracy mass cytometry provides, variations in the detection of the signal in the different mass channels can still lead to some inaccurate receptor occupancy estimations. In fact, Bringeland et al. (2019) showed an overestimation of receptor occupancy when the drug was conjugated to a metal detected by a more sensitive channel than that of the receptors [70]. Their solution was to use QSC beads, consisting of different microspheres populations binding an increasing number of antibodies in each bead population. QSC beads are normally used in flow cytometry, and the detection of all the populations was not achieved with the normal protocol. Therefore, an adjusted protocol was used, where the beads was coated with OsO_4 before being stained with the conjugated antibody. The work conducted by Bringeland et al. (2019) was done on a Helios® (Fluidigm, South San Fransisco, CA, USA), while the work in this thesis was exclusively run on a CyTOF XT®, a newer generation of the Fluidigm mass cytometers. Due to the workload and safety hazard associated with using OsO_4, we wanted to test if the sensitivity of CyTOF XT® was sufficient to detect 166Er-anti-PD-1 [EH12.1] in all the populations.

From Figure 4.12 b) we can see that there is a difference in the amount of bound 166Er-anti-PD-1 [EH12.1] (y-axis) between beads 3 and 4, but beads 1 and 2 are not distinguishable from bead 3. Without the distinct signal associated with the lower bead populations, it is not possible to create a standard curve from the measurements. Hence, the beads cannot be used for standardization of the receptor occupancy measurements in this thesis. Budzinski et al. (2019) argue that QSC beads are not detected on a mass cytometer due to lacking a metal isotope label [82]. In flow cytometry, the beads are detected by the light scatter and/or inherent fluorescence emitted by the beads themselves, while the light emitted by the fluorescence from the labeled antibodies are detected in a separate channel. Mass cytometry has no equivalent feature to detect the beads themselves and is dependent on the signal from the metals conjugated to the antibodies to detect each bead population. The results in Figure 4.12 b) show that beads 3 and 4 are close to the event length detection limit of the mass cytometer. It could certainly be that the lower bead populations simply do not have enough metal isotopes on them to be detected by the mass cytometer. The authors of the paper are the ones who developed the protocol using OsO_4 to coat the beads, enabling the beads to be detected independently of the signal from the antibodies [82].

This thesis showed that using QSC beads on CyTOF XT® still does not provide sufficient sensitivity for detecting all the bead populations (see Figures 4.10 and 4.12). To optimize the receptor occupancy assay described in this thesis, implementing the OsO_4-protocol for using QSC beads could be of interest. Despite a quite time-consuming process and the hazard risk associated with using OsO_4, coating the QSC beads will enable the standardization of the signals used for calculating the receptor occupancy. Even though Budzinski et al. (2019) report that they obtained ABC (Antibodies Bound per Cell) values were mostly consistent with published data on the expected number of epitopes, it is still unknown if ABC values can be derived from the signals in mass cytometry. Osmium has been reported to directly bind to the lipids in the cell membrane. Since the beads are coated before the staining with antibodies, it is still unknown if this effects the number of antibodies that can bind to each bead.

If converting the signal to a number of ABC was possible, it would drastically improve the accuracy of the receptor occupancy estimates. But the standardization from using the QSC beads would still make it possible to compare the signal from one channel to that of another. This would enable the 173Yb-anti-IgG4 [HP6025] signals to be divided by the 166Er-anti-PD-1 [EH12.1] signal of the first sample (detecting all available receptors). This would provide absolute receptor occupancy percentages instead of relative ones. In this case, the increasing signal of bound pembrolizumab (173Yb-anti-IgG4 [HP6025]) could be compared to the decreasing signal of available PD-1 receptors (166Er-anti-PD-1 [EH12.1]) to check whether they correspond or not. Lastly, the standardization provided by the beads would also increase the repeatability and reproducibility, both intra- and inter-laboratory, of the receptor occupancy measurements. Implementing OsO_4 coated QSC beads in the receptor occupancy assay of this thesis would, therefore, be beneficial.

5.3 Receptor Occupancy as a Predictive Biomarker

We hypothesized that the receptor occupancy of pembrolizumab could contribute to predict if the patient was a responder or non-responder. The general pattern for all the patients is that the receptor occupancy on PD-1 by pembrolizumab seems to increase throughout treatment, seen as a decrease in the binding of 166Er-anti-PD-1 [EH12.1] and an increase in the binding of 173Yb-anti-IgG4 [HP6025] in Figure 4.8 d). Figure 4.9 shows that there exist variations between the patients in the pattern of how the binding of antibodies changes with time. To better visualize how the receptor occupancy was changing with time within each patient, a selection of the three patients with the most collected samples (Patients 13, 14 and 17) was displayed in Figure 4.10.

Patient 17 had two RECIST-evaluations that both stated progressive and was considered a non-responder in this thesis. Patient 13 had partial regression in a RECIST-evaluation conducted 60 days (approximately nine weeks) after first injection and was considered a responder. This patient eventually had progressive RECIST-evaluation as well, but this evaluation was conducted 511 days after start of treatment (corresponding to around 73 weeks after treatment start). The last samples available for this patient was collected at week 40. Patient 14 was also categorized as a responder due to first evaluation being stable disease and eventually experiencing complete remission after 764 days (around 110 weeks). The difference in the pattern of 173Yb-anti-IgG4 [HP6025] signal between the patients is striking. While the non-responder has little to no change in receptor occupancy with time, the responders have a clear increase in the binding of 173Yb-anti-IgG4 [HP6025] already 2 hours after injection. The curve of the two responders seems to follow the same pattern as an expected serum concentration-time curve for pembrolizumab [83] . However, three patients are undoubtedly insufficient to state anything about a correlation to response. In addition, the level of bound 166Er-anti-PD-1 [EH12.1] actually seems to drop more significantly in patient 17 than in the other two patients, contradicting the observations seen about 173Yb-anti-IgG4 [HP6025].

According to the preliminary statistical analysis performed in section 4.3.3, the receptor occupancy estimates from this thesis does not seem to be able to distinguish a responder and non-responder. There are several limitations in the data for this thesis that could influence the outcome of the preliminary statistical analysis that was performed. Firstly, the main limitation is that the number of patients (n=9) included in the analysis is very low. The lack of longitudinal data for many of the patients is also a challenge. Not only does it limit the timepoints that can be used in the statistical analysis, but it also complicates the process of categorizing responders and non-responders, as both evaluations were done after the last sample collection for several patients. If more longitudinal samples were available, statistical analysis like Spearman could also have been used to assess the question of receptor occupancy as predictor of response.

Another limitation is the simplified process of defining responders and non-responders. Only having two categories might be inadequate for this investigative issue. It is hard to say if the patients who died before any RECIST-evaluations was conducted did respond or not. Ideally, these patients should have been excluded from the statistical analysis, but they were included since the number of patients were already low. Alternatively, the patients could have been categorized as non-responders if they had progressive disease, stable if they had stable disease,

and responders if they experienced partial regression or complete remission. Then, a statistical analysis like ANOVA could have been employed. Lastly, there was only conducted one statistical analysis. A t-test only tests if there is any significant difference in the mean between two datasets. Complementing the statistical analyses with other statistical methods like ANOVA, Spearman as mentioned in this paragraph could give more confidence in answering if receptor occupancy of pembrolizumab can serve as a predictive biomarker.

The current standard for identifying patients likely to respond to treatment with pembrolizumab is the expression of PD-L1 on tumor cells by immunohistochemistry. However, there was only a 44,8% response rate in the KEYNOTE 024 trails even though all patients included had PD-L1 expression on more than 50% of the tumor cells (shown to be related to response) [84]. It is obvious that the PD-L1 expression alone is insufficient as a predictive biomarker. Other biomarkers shown to be associated with response has been proposed but are currently also inadequate to be use alone [85], [86]. The receptor occupancy of pembrolizumab did not seem to predict response of the patients in this thesis, but more patients and optimization of the assay is necessary to properly conclude on this topic. Likely, receptor occupancy alone cannot be used to predict the response to pembrolizumab for all patients but could complement the other suggested predictive biomarkers. The combination of several biomarkers could possibly improve response prediction, resulting in better patient selection for treatment. This would both save unnecessary costs and treatments, resulting in better patient care.

6 Concluding Remarks and Future Perspectives

This thesis aimed to develop a mass cytometry assay to measure the PD-1 receptor occupancy by pembrolizumab. A mass cytometry panel was successfully developed, using 173Yb-anti-IgG4 [HP6025] to detect bound pembrolizumab and 166Er-anti-PD-1 [EH12.1] to detect available receptors not bound by pembrolizumab. We hypothesized that measuring the receptor occupancy on PD-1 by pembrolizumab could identify responders from non-responders. The occupation by pembrolizumab was expected to increase throughout treatment, which we were able to verify using the assay.

According to a preliminary statistical analysis, there was no clear difference between the receptor occupancy measured in responders and non-responders 2 hours after injection with pembrolizumab. More patients are needed to properly address if there is a relation between PD-1 receptor occupancy and response. Further studies are also required to assess the effect fixation has on the receptor occupancy quantification. In addition, the implementation of beads to standardize the measurements would both improve the accuracy and enable the measurements of bound and available receptors to be compared with each other. Still, this assay is the first measuring receptor occupancy on PD-1 that utilizes mass cytometry. Because of the assay's ability to investigate multiple cell populations simultaneously, it could potentially serve as a valuable addition in predicting response for pembrolizumab treated patients.

References

[1] D. M. Pardoll, 'The blockade of immune checkpoints in cancer immunotherapy', *Nat. Rev. Cancer*, vol. 12, no. 4, Art. no. 4, Apr. 2012, doi: 10.1038/nrc3239.

[2] J. Gong, A. Chehrazi-Raffle, S. Reddi, and R. Salgia, 'Development of PD-1 and PD-L1 inhibitors as a form of cancer immunotherapy: a comprehensive review of registration trials and future considerations', *J. Immunother. Cancer*, vol. 6, p. 8, Jan. 2018, doi: 10.1186/s40425-018-0316-z.

[3] 'Keytruda : EPAR - All authorised presentation'. European Medicines Agency, Jul. 30, 2015. [Online]. Available: https://www.ema.europa.eu/en/documents/product-information/keytruda-epar-product-information_en.pdf

[4] E. B. Garon *et al.*, 'Pembrolizumab for the Treatment of Non–Small-Cell Lung Cancer', *N. Engl. J. Med.*, vol. 372, no. 21, pp. 2018–2028, May 2015, doi: 10.1056/NEJMoa1501824.

[5] P. Darvin, S. M. Toor, V. Sasidharan Nair, and E. Elkord, 'Immune checkpoint inhibitors: recent progress and potential biomarkers', *Exp. Mol. Med.*, vol. 50, no. 12, Art. no. 12, Dec. 2018, doi: 10.1038/s12276-018-0191-1.

[6] G. T. Gibney, L. M. Weiner, and M. B. Atkins, 'Predictive biomarkers for checkpoint inhibitor-based immunotherapy', *Lancet Oncol.*, vol. 17, no. 12, pp. e542–e551, Dec. 2016, doi: 10.1016/S1470-2045(16)30406-5.

[7] A. K. Abbas, A. H. Lichtman, and S. Pillai, *Basic immunology: functions and disorders of the immune system*, Sixth edition. Philadelphia, PA: Elsevier, 2020.

[8] H. W. Schroeder and L. Cavacini, 'Structure and Function of Immunoglobulins', *J. Allergy Clin. Immunol.*, vol. 125, no. 2 0 2, pp. S41–S52, Feb. 2010, doi: 10.1016/j.jaci.2009.09.046.

[9] A. K. Abbas, A. H. Lichtman, S. Pillai, and D. L. Baker, *Cellular and molecular immunology*, Tenth edition. Philadelphia, Pennsylvania: Elsevier, 2022.

[10] J. Charles A Janeway, P. Travers, M. Walport, and M. J. Shlomchik, 'The structure of a typical antibody molecule', in *Immunobiology: The Immune System in Health and Disease. 5th edition*, Garland Science, 2001. Accessed: May 01, 2023. [Online]. Available: https://www.ncbi.nlm.nih.gov/books/NBK27144/

[11] M. L. Chiu, D. R. Goulet, A. Teplyakov, and G. L. Gilliland, 'Antibody Structure and Function: The Basis for Engineering Therapeutics', *Antibodies*, vol. 8, no. 4, p. 55, Dec. 2019, doi: 10.3390/antib8040055.

[12] I. Sela-Culang, V. Kunik, and Y. Ofran, 'The structural basis of antibody-antigen recognition', *Front. Immunol.*, vol. 4, p. 302, Oct. 2013, doi: 10.3389/fimmu.2013.00302.

[13] 'Difference Between a Paratope and an Epitope', *News-Medical.net*, Feb. 14, 2020. https://www.azolifesciences.com/article/Difference-Between-a-Paratope-and-an-Epitope.aspx (accessed May 24, 2023).

[14] C. Chothia and A. M. Lesk, 'Canonical structures for the hypervariable regions of immunoglobulins', *J. Mol. Biol.*, vol. 196, no. 4, pp. 901–917, Aug. 1987, doi: 10.1016/0022-2836(87)90412-8.

[15] F. Nimmerjahn and J. V. Ravetch, 'Fcγ receptors as regulators of immune responses', *Nat. Rev. Immunol.*, vol. 8, no. 1, Art. no. 1, Jan. 2008, doi: 10.1038/nri2206.

[16] P. Funfrock, 'How humanized antibodies revolutionized drug development', *ProteoGenix*, Sep. 04, 2019. https://www.proteogenix.science/scientific-corner/antibody-production/humanized-antibody-therapeutic-applications/ (accessed May 24, 2023).

[17] M. H. Andersen, D. Schrama, P. thor Straten, and J. C. Becker, 'Cytotoxic T Cells', *J. Invest. Dermatol.*, vol. 126, no. 1, pp. 32–41, Jan. 2006, doi: 10.1038/sj.jid.5700001.

[18] B. Alberts, A. Johnson, J. Lewis, M. Raff, K. Roberts, and P. Walter, 'Helper T Cells and Lymphocyte Activation', *Mol. Biol. Cell 4th Ed.*, 2002, Accessed: Apr. 14, 2023. [Online]. Available: https://www.ncbi.nlm.nih.gov/books/NBK26827/

[19] S. Sakaguchi, T. Yamaguchi, T. Nomura, and M. Ono, 'Regulatory T Cells and Immune Tolerance', *Cell*, vol. 133, no. 5, pp. 775–787, May 2008, doi: 10.1016/j.cell.2008.05.009.

[20] N. H. Overgaard, J.-W. Jung, R. J. Steptoe, and J. W. Wells, 'CD4+/CD8+ double-positive T cells: more than just a developmental stage?', *J. Leukoc. Biol.*, vol. 97, no. 1, pp. 31–38, Jan. 2015, doi: 10.1189/jlb.1RU0814-382.

[21] E. E. Hillhouse and S. Lesage, ‘A comprehensive review of the phenotype and function of antigen-specific immunoregulatory double negative T cells’, *J. Autoimmun.*, vol. 40, pp. 58–65, Feb. 2013, doi: 10.1016/j.jaut.2012.07.010.
[22] A. D. Waldman, J. M. Fritz, and M. J. Lenardo, ‘A guide to cancer immunotherapy: from T cell basic science to clinical practice’, *Nat. Rev. Immunol.*, vol. 20, no. 11, Art. no. 11, Nov. 2020, doi: 10.1038/s41577-020-0306-5.
[23] N. D. Pennock, J. T. White, E. W. Cross, E. E. Cheney, B. A. Tamburini, and R. M. Kedl, ‘T cell responses: naïve to memory and everything in between’, *Adv. Physiol. Educ.*, vol. 37, no. 4, pp. 273–283, Dec. 2013, doi: 10.1152/advan.00066.2013.
[24] F. Sallusto, J. Geginat, and A. Lanzavecchia, ‘Central Memory and Effector Memory T Cell Subsets: Function, Generation, and Maintenance’, *Annu. Rev. Immunol.*, vol. 22, no. 1, pp. 745–763, 2004, doi: 10.1146/annurev.immunol.22.012703.104702.
[25] Y. Agata *et al.*, ‘Expression of the PD-1 antigen on the surface of stimulated mouse T and B lymphocytes’, *Int. Immunol.*, vol. 8, no. 5, pp. 765–772, May 1996, doi: 10.1093/intimm/8.5.765.
[26] Y. Ishida, Y. Agata, K. Shibahara, and T. Honjo, ‘Induced expression of PD-1, a novel member of the immunoglobulin gene superfamily, upon programmed cell death.’, *EMBO J.*, vol. 11, no. 11, pp. 3887–3895, Nov. 1992.
[27] L. M. Francisco, P. T. Sage, and A. H. Sharpe, ‘The PD-1 Pathway in Tolerance and Autoimmunity’, *Immunol. Rev.*, vol. 236, pp. 219–242, Jul. 2010, doi: 10.1111/j.1600-065X.2010.00923.x.
[28] T. Okazaki and T. Honjo, ‘PD-1 and PD-1 ligands: from discovery to clinical application’, *Int. Immunol.*, vol. 19, no. 7, pp. 813–824, Jul. 2007, doi: 10.1093/intimm/dxm057.
[29] T. Yamazaki *et al.*, ‘Expression of Programmed Death 1 Ligands by Murine T Cells and APC1’, *J. Immunol.*, vol. 169, no. 10, pp. 5538–5545, Nov. 2002, doi: 10.4049/jimmunol.169.10.5538.
[30] G. J. Freeman *et al.*, ‘Engagement of the Pd-1 Immunoinhibitory Receptor by a Novel B7 Family Member Leads to Negative Regulation of Lymphocyte Activation’, *J. Exp. Med.*, vol. 192, no. 7, pp. 1027–1034, Oct. 2000.
[31] Y. Iwai, M. Ishida, Y. Tanaka, T. Okazaki, T. Honjo, and N. Minato, ‘Involvement of PD-L1 on tumor cells in the escape from host immune system and tumor immunotherapy by PD-L1 blockade’, *Proc. Natl. Acad. Sci.*, vol. 99, no. 19, pp. 12293–12297, Sep. 2002, doi: 10.1073/pnas.192461099.
[32] R. Hino *et al.*, ‘Tumor cell expression of programmed cell death-1 ligand 1 is a prognostic factor for malignant melanoma’, *Cancer*, vol. 116, no. 7, pp. 1757–1766, Apr. 2010, doi: 10.1002/cncr.24899.
[33] S. Muenst *et al.*, ‘Expression of programmed death ligand 1 (PD-L1) is associated with poor prognosis in human breast cancer’, *Breast Cancer Res. Treat.*, vol. 146, no. 1, pp. 15–24, Jul. 2014, doi: 10.1007/s10549-014-2988-5.
[34] L. Fashoyin-Aje *et al.*, ‘FDA Approval Summary: Pembrolizumab for Recurrent Locally Advanced or Metastatic Gastric or Gastroesophageal Junction Adenocarcinoma Expressing PD-L1’, *The Oncologist*, vol. 24, no. 1, pp. 103–109, Jan. 2019, doi: 10.1634/theoncologist.2018-0221.
[35] C. J. Maine *et al.*, ‘Programmed death ligand-1 over-expression correlates with malignancy and contributes to immune regulation in ovarian cancer’, *Cancer Immunol. Immunother. CII*, vol. 63, no. 3, pp. 215–224, Mar. 2014, doi: 10.1007/s00262-013-1503-x.
[36] Z. Zeng *et al.*, ‘Upregulation of circulating PD-L1/PD-1 is associated with poor post-cryoablation prognosis in patients with HBV-related hepatocellular carcinoma’, *PloS One*, vol. 6, no. 9, p. e23621, 2011, doi: 10.1371/journal.pone.0023621.
[37] R. H. Thompson *et al.*, ‘Tumor B7-H1 is associated with poor prognosis in renal cell carcinoma patients with long-term follow-up’, *Cancer Res.*, vol. 66, no. 7, pp. 3381–3385, Apr. 2006, doi: 10.1158/0008-5472.CAN-05-4303.
[38] T. Nomi *et al.*, ‘Clinical significance and therapeutic potential of the programmed death-1 ligand/programmed death-1 pathway in human pancreatic cancer’, *Clin. Cancer Res. Off. J. Am. Assoc. Cancer Res.*, vol. 13, no. 7, pp. 2151–2157, Apr. 2007, doi: 10.1158/1078-0432.CCR-06-2746.

[39] B. A. Inman *et al.*, 'PD-L1 (B7-H1) expression by urothelial carcinoma of the bladder and BCG-induced granulomata: associations with localized stage progression', *Cancer*, vol. 109, no. 8, pp. 1499–1505, Apr. 2007, doi: 10.1002/cncr.22588.
[40] D. Y. Lin *et al.*, 'The PD-1/PD-L1 complex resembles the antigen-binding Fv domains of antibodies and T cell receptors', *Proc. Natl. Acad. Sci. U. S. A.*, vol. 105, no. 8, pp. 3011–3016, Feb. 2008, doi: 10.1073/pnas.0712278105.
[41] K. M. Zak *et al.*, 'Structure of the Complex of Human Programmed Death 1, PD-1, and Its Ligand PD-L1', *Struct. Lond. Engl. 1993*, vol. 23, no. 12, pp. 2341–2348, Dec. 2015, doi: 10.1016/j.str.2015.09.010.
[42] Z. Na *et al.*, 'Structural basis for blocking PD-1-mediated immune suppression by therapeutic antibody pembrolizumab', *Cell Res.*, vol. 27, no. 1, Art. no. 1, Jan. 2017, doi: 10.1038/cr.2016.77.
[43] J. Y. Lee *et al.*, 'Structural basis of checkpoint blockade by monoclonal antibodies in cancer immunotherapy', *Nat. Commun.*, vol. 7, p. 13354, Oct. 2016, doi: 10.1038/ncomms13354.
[44] S. Horita, Y. Nomura, Y. Sato, T. Shimamura, S. Iwata, and N. Nomura, 'High-resolution crystal structure of the therapeutic antibody pembrolizumab bound to the human PD-1', *Sci. Rep.*, vol. 6, no. 1, Art. no. 1, Oct. 2016, doi: 10.1038/srep35297.
[45] P. Fessas, H. Lee, S. Ikemizu, and T. Janowitz, 'A molecular and preclinical comparison of the PD-1–targeted T-cell checkpoint inhibitors nivolumab and pembrolizumab', *Semin. Oncol.*, vol. 44, no. 2, pp. 136–140, Apr. 2017, doi: 10.1053/j.seminoncol.2017.06.002.
[46] 'ISAC - What is Cytometry?' https://isac-net.org/page/What-is-Cytometry (accessed May 18, 2023).
[47] 'Flow cytometry introduction | Abcam'. https://www.abcam.com/protocols/introduction-to-flow-cytometry (accessed May 18, 2023).
[48] K. M. McKinnon, 'Flow Cytometry: An Overview', *Curr. Protoc. Immunol.*, vol. 120, p. 5.1.1-5.1.11, Feb. 2018, doi: 10.1002/cpim.40.
[49] A. Adan, G. Alizada, Y. Kiraz, Y. Baran, and A. Nalbant, 'Flow cytometry: basic principles and applications', *Crit. Rev. Biotechnol.*, vol. 37, no. 2, pp. 163–176, Feb. 2017, doi: 10.3109/07388551.2015.1128876.
[50] 'Flow Cytometry Basics, FACS Priciple. How Does Flow Cytometry Work', *Bosterbio*. https://www.bosterbio.com/protocol-and-troubleshooting/flow-cytometry-principle (accessed May 18, 2023).
[51] M. H. Spitzer and G. P. Nolan, 'Mass Cytometry: Single Cells, Many Features', *Cell*, vol. 165, no. 4, pp. 780–791, May 2016, doi: 10.1016/j.cell.2016.04.019.
[52] S. C. Bendall *et al.*, 'Single-cell mass cytometry of differential immune and drug responses across a human hematopoietic continuum', *Science*, vol. 332, no. 6030, pp. 687–696, May 2011, doi: 10.1126/science.1198704.
[53] S. C. Bendall, G. P. Nolan, M. Roederer, and P. K. Chattopadhyay, 'A deep profiler's guide to cytometry', *Trends Immunol.*, vol. 33, no. 7, pp. 323–332, Jul. 2012, doi: 10.1016/j.it.2012.02.010.
[54] L. R. Olsen, M. D. Leipold, C. B. Pedersen, and H. T. Maecker, 'The anatomy of single cell mass cytometry data', *Cytom. Part J. Int. Soc. Anal. Cytol.*, vol. 95, no. 2, pp. 156–172, Feb. 2019, doi: 10.1002/cyto.a.23621.
[55] G. K. Behbehani *et al.*, 'Transient partial permeabilization with saponin enables cellular barcoding prior to surface marker staining', *Cytom. Part J. Int. Soc. Anal. Cytol.*, vol. 85, no. 12, pp. 1011–1019, Dec. 2014, doi: 10.1002/cyto.a.22573.
[56] Z. B. Bjornson, G. P. Nolan, and W. J. Fantl, 'Single-cell mass cytometry for analysis of immune system functional states', *Curr. Opin. Immunol.*, vol. 25, no. 4, pp. 484–494, Aug. 2013, doi: 10.1016/j.coi.2013.07.004.
[57] D. C. Harris and C. A. Lucy, *Quantitative chemical analysis*, Tenth edition. Austin: Macmillan Learning, 2020.
[58] P. Ehrlich, 'Croonian lecture.—On immunity with special reference to cell life', *Proc. R. Soc. Lond.*, vol. 66, no. 424–433, pp. 424–448, Jan. 1900, doi: 10.1098/rspl.1899.0121.
[59] S. C. Cowles *et al.*, 'An affinity threshold for maximum efficacy in anti-PD-1 immunotherapy', *mAbs*, vol. 14, no. 1, p. 2088454, Dec. 2022, doi: 10.1080/19420862.2022.2088454.

[60] J. J. Stewart *et al.*, 'Role of receptor occupancy assays by flow cytometry in drug development', *Cytometry B Clin. Cytom.*, vol. 90, no. 2, pp. 110–116, 2016, doi: 10.1002/cyto.b.21355.
[61] C. L. Green *et al.*, 'Recommendations for the development and validation of flow cytometry-based receptor occupancy assays', *Cytometry B Clin. Cytom.*, vol. 90, no. 2, pp. 141–149, 2016, doi: 10.1002/cyto.b.21339.
[62] K. Huse, 'Expanding the Clinical Cytometry Toolbox—Receptor Occupancy by Mass Cytometry', *Cytometry A*, vol. 95, no. 10, pp. 1046–1048, 2019, doi: 10.1002/cyto.a.23784.
[63] J. R. Brahmer *et al.*, 'Phase I Study of Single-Agent Anti–Programmed Death-1 (MDX-1106) in Refractory Solid Tumors: Safety, Clinical Activity, Pharmacodynamics, and Immunologic Correlates', *J. Clin. Oncol.*, vol. 28, no. 19, pp. 3167–3175, Jul. 2010, doi: 10.1200/JCO.2009.26.7609.
[64] S. L. Topalian *et al.*, 'Safety, Activity, and Immune Correlates of Anti–PD-1 Antibody in Cancer', *N. Engl. J. Med.*, vol. 366, no. 26, pp. 2443–2454, Jun. 2012, doi: 10.1056/NEJMoa1200690.
[65] D. Pluim, W. Ros, I. H. C. Miedema, J. H. Beijnen, and J. H. M. Schellens, 'Multiparameter Flow Cytometry Assay for Quantification of Immune Cell Subsets, PD-1 Expression Levels and PD-1 Receptor Occupancy by Nivolumab and Pembrolizumab', *Cytometry A*, vol. 95, no. 10, pp. 1053–1065, 2019, doi: 10.1002/cyto.a.23873.
[66] J. Fu *et al.*, 'Receptor occupancy measurement of anti-PD-1 antibody drugs in support of clinical trials', *Bioanalysis*, vol. 11, no. 14, pp. 1347–1358, Jul. 2019, doi: 10.4155/bio-2019-0090.
[67] A. Osa *et al.*, 'Clinical implications of monitoring nivolumab immunokinetics in non–small cell lung cancer patients', *JCI Insight*, vol. 3, no. 19, p. e59125, doi: 10.1172/jci.insight.59125.
[68] A. Osa *et al.*, 'Monitoring antibody binding to T cells in a pembrolizumab-treated patient with lung adenocarcinoma on hemodialysis', *Thorac. Cancer*, vol. 10, no. 11, pp. 2183–2187, Nov. 2019, doi: 10.1111/1759-7714.13197.
[69] M. Gazzano *et al.*, 'Anti-PD-1 immune-related adverse events are associated with high therapeutic antibody fixation on T cells', *Front. Immunol.*, vol. 13, p. 1082084, 2022, doi: 10.3389/fimmu.2022.1082084.
[70] G. H. Bringeland *et al.*, 'Optimization of Receptor Occupancy Assays in Mass Cytometry: Standardization Across Channels with QSC Beads', *Cytom. Part J. Int. Soc. Anal. Cytol.*, vol. 95, no. 3, pp. 314–322, Mar. 2019, doi: 10.1002/cyto.a.23723.
[71] C. R. Stevens, K. Atkuri, D. L. Menard, L. E. King, H. Neubert, and P. Goihberg, 'Mass-cytometry for the multiplexed quantification and characterization of target expression on circulating cells in whole blood', *Cytometry A*, vol. n/a, no. n/a, doi: 10.1002/cyto.a.24730.
[72] S.-E. Gullaksen *et al.*, 'Titrating Complex Mass Cytometry Panels', *Cytometry A*, vol. 95, no. 7, pp. 792–796, 2019, doi: 10.1002/cyto.a.23751.
[73] N. Kotecha, P. O. Krutzik, and J. M. Irish, 'Web-based analysis and publication of flow cytometry experiments', *Curr. Protoc. Cytom.*, vol. Chapter 10, p. Unit10.17, Jul. 2010, doi: 10.1002/0471142956.cy1017s53.
[74] W. Yang, P. W. Chen, H. Li, H. Alizadeh, and J. Y. Niederkorn, 'PD-L1: PD-1 Interaction Contributes to the Functional Suppression of T-Cell Responses to Human Uveal Melanoma Cells In Vitro', *Invest. Ophthalmol. Vis. Sci.*, vol. 49, no. 6, pp. 2518–2525, Jun. 2008, doi: 10.1167/iovs.07-1606.
[75] C. B. Bagwell *et al.*, 'Automated Data Cleanup for Mass Cytometry', *Cytometry A*, vol. 97, no. 2, pp. 184–198, 2020, doi: 10.1002/cyto.a.23926.
[76] H. L. Crowell, V. R. T. Zanotelli, S. Chevrier, and M. D. Robinson, 'CATALYST: Cytometry dATa anALYSis'. 2022. [Online]. Available: https://github.com/HelenaLC/CATALYST
[77] S. Van Gassen *et al.*, 'FlowSOM: Using self-organizing maps for visualization and interpretation of cytometry data', *Cytometry A*, vol. 87A, no. 7, pp. 636–645, Jul. 2015, doi: 10.1002/cyto.a.22625.
[78] L. McInnes, J. Healy, and J. Melville, 'UMAP: Uniform Manifold Approximation and Projection for Dimension Reduction'. arXiv, Feb. 09, 2018. doi: 10.48550/arXiv.1802.03426.
[79] H. Wickham, *ggplot2: Elegant Graphics for Data Analysis*, 2nd ed. 2016. in Use R! Cham: Springer International Publishing : Imprint: Springer, 2016. doi: 10.1007/978-3-319-24277-4.

[80] G. H. Bringeland, N. Blaser, K.-M. Myhr, C. A. Vedeler, and S. Gavasso, 'Wearing-off at the end of natalizumab dosing intervals is associated with low receptor occupancy', *Neurol. - Neuroimmunol. Neuroinflammation*, vol. 7, no. 3, May 2020, doi: 10.1212/NXI.0000000000000678.
[81] Z. L. E. van Kempen *et al.*, 'The natalizumab wearing-off effect: End of natalizumab cycle, recurrence of MS symptoms', *Neurology*, vol. 93, no. 17, pp. e1579–e1586, Oct. 2019, doi: 10.1212/WNL.0000000000008357.
[82] L. Budzinski *et al.*, 'Osmium-Labeled Microspheres for Bead-Based Assays in Mass Cytometry', *J. Immunol.*, vol. 202, no. 10, pp. 3103–3112, May 2019, doi: 10.4049/jimmunol.1801640.
[83] M. Ahamadi *et al.*, 'Model-Based Characterization of the Pharmacokinetics of Pembrolizumab: A Humanized Anti–PD-1 Monoclonal Antibody in Advanced Solid Tumors', *CPT Pharmacomet. Syst. Pharmacol.*, vol. 6, no. 1, pp. 49–57, 2017, doi: 10.1002/psp4.12139.
[84] M. Reck *et al.*, 'Pembrolizumab versus Chemotherapy for PD-L1–Positive Non–Small-Cell Lung Cancer', *N. Engl. J. Med.*, vol. 375, no. 19, pp. 1823–1833, Nov. 2016, doi: 10.1056/NEJMoa1606774.
[85] D. R. Camidge, R. C. Doebele, and K. M. Kerr, 'Comparing and contrasting predictive biomarkers for immunotherapy and targeted therapy of NSCLC', *Nat. Rev. Clin. Oncol.*, vol. 16, no. 6, Art. no. 6, Jun. 2019, doi: 10.1038/s41571-019-0173-9.
[86] J. N. Bodor, Y. Boumber, and H. Borghaei, 'Biomarkers for immune checkpoint inhibition in non–small cell lung cancer (NSCLC)', *Cancer*, vol. 126, no. 2, pp. 260–270, 2020, doi: 10.1002/cncr.32468.
[87] T. Inoue, A. Swain, Y. Nakanishi, and D. Sugiyama, 'Multicolor Analysis of Cell Surface Marker of Human Leukemia Cell Lines Using Flow Cytometry', *Anticancer Res.*, vol. 34, no. 8, pp. 4539–4550, Aug. 2014.